東海大学大学院令和元年度博士論文

Dielectric study and evaluation of water structures on various scales *in vivo* and *in vitro*

（多様なスケールにおける *in vivo* および *in vitro* の
水構造に関する誘電的研究と評価）

指導　　八木原　晋　　教授

東海大学大学院総合理工学研究科

総合理工学専攻

丸山　裕子

Preface

This thesis is written as a doctoral dissertation presented to the Graduate School of Science and Technology of Tokai University titled "Dielectric study and evaluation of water structures on various scales *in vivo* and *in vitro*".

Various biological functions are closely related to the existence state of water with the dynamics of water molecules included in materials. But it hasn't been clearly understood yet to interpret physical properties and life phenomena because of difficulties in observations of dynamic behaviors of water molecules. Interpretations focusing on the dynamic behaviors of water molecules is then still important in a wide range of research fields.

In this study, the molecular mechanism was elucidated by universal interpretation focusing on water structures on various scales *in vivo* and *in vitro* for regarding the physical properties and functions of biological models organized across the hierarchy from the molecular level to the organizational level using broadband dielectric spectroscopy in the frequency region from 10 MHz up to 65 GHz, and the validity of the physical properties and function evaluation applied to it was discussed.

This doctor's thesis is organized as follows;

In chapter 1, the background and purpose of this study were explained with basic matters.

In chapter 2, the principle of the measurement method used for the observation of molecular motions and the details of the actual measurement method were explained.

In chapter 3, dielectric relaxation and diffusion coefficient measurements by nuclear magnetic resonance (NMR) methods were discussed for protein-water mixtures and cheeses. The τ–β diagram analyzed these aqueous systems and cheese suggested that the hydrogen-bonded network of water structures in cheese is dispersed with the higher fractal dimensions than those of protein solutions, since various biomolecules coexist with the gel of proteins in cheese. The fractal analysis using the τ–β diagram was effective to characterize those water structures.

In chapter 4, the penetration depth of the fringing field from open-ended coaxial probes with different diameters were characterized from TDR measurements applied to the acetone-Teflon double-layer dielectric model. The penetration depth increases with increasing electrode diameter. Water structures in vivo was also evaluated by dielectric measurements on the human skin, using the penetration depth thus obtained from the measurements for the double-layer dielectric model. Skin measurements on various parts were carried out for two examinees with five types of electrode diameters, and the results reflected the thickness of the examinee's epidermis. This methodology suggests an effective method of detailed evaluations for the human skin.

In chapter 5, Biological blood flow was observed by dielectric spectroscopy, ultrasonic blood flow

meter, and laser blood flow meter. Detailed results in dielectric relaxation measurements confirmed that the relaxation process increased immediately after a sprint in the 1 MHz region where the relaxation of interface polarization dominantly from red blood cells was observed when the blood flow before and after sprint of two examinees. Similarly, results from ultrasonic blood flow measurements are compared with the relaxation strength, and it was found that blood vessels dilated by sprint and the blood flow velocity slowed. The measurements by the laser blood flow meter also showed that the blood volume corresponding to the red blood cell number density increased immediately after the sprint. These results of the dielectric measurements, the laser blood flow meter, and the ultrasonic blood flow measurements were well corresponded for red blood cells. Dielectric spectroscopy was able to confirm the state of blood *in vivo*, suggesting the usefulness of blood measurement.

In chapter 6, the summary of this thesis and new findings obtained here are organized.

The results obtained in this thesis are likely to lead to the developments for the future research in biological systems. The present water structure analysis is not limited to biological systems, and it is expected to expand understanding in various research fields in the future.

Acknowledgments

First and foremost, I would like to express my heartfelt gratitude to my supervisor, Professor Shin Yagihara, for his constant encouragement and guidance on my research. He not only gives me consistent and illuminating instruction in research but also acts as an example who is responsible and devoted to research.

I am deeply indebted to Professor Rio Kita, Professor Naoki Shinyashiki and Professor Minoru Fukuzaki for the insightful comment, which help me improving and extending my research.

I would like to thank Associate Professor Haruchika Masuda, School of Medicine, Tokai University, who has been very busy reviewing this doctoral thesis and has received many advices.

I would like to thank all of the members of our research group (RGMS: Research Group of Molecular complex Systems of Tokai University).

I am grateful also to my family for their understandings and encouragements, especially my son Ryosuke.

CONTENTS

Chapter 1

Introduction

1.1 Background and purpose

The various biological functions are closely related to the state of water and especially to dynamic behaviors of water molecules. There still remains serious ambiguities, however, in interpretations of physical properties and life phenomena focusing on the dynamic behaviors of water molecules because of difficulties in observation and analytical techniques for the water molecules and those aggregation structures. Then interpretation focusing on dynamic behaviors of water molecules is still one of the most important subjects in a wide range of research fields including applied researches as well as fundamental researches.

Water molecules behaves with cooperative Brownian motion, repeating hydrogen bond breaking and recombination. Previous studies of our research group (RGMS: Research Group of Molecular complex Systems of Tokai University) [1] has suggested that the dynamic behaviors of water molecules are interpreted as a dynamic cluster structure with an average of 5 to 6 water molecules and/or the dynamic behavior of the hydrogen bonded network due to the rate process of generation and corruption of hydrogen bonds with the correlation length. Dielectric studies on pure water shows that dynamic behaviors of water molecules are observed as Debye-type single relaxation process with the relaxation time τ of 8.27 ps at 25 °C [2-5]. The relaxation time is a characteristic time for the rotational diffusion of molecules, while the presence of a small relaxation process reflecting more local dynamics has been reported in one or more-digit higher frequency range of THz region. The elementary process of breaking and recombination of hydrogen bonds among molecules may be closely related to this THz frequency process, however, a detailed discussion of this has yet to be completed. In the case of water-mixed systems, dynamic behaviors are characterized by slow dynamics with a delay in the average dynamics of water molecules and a broadening of the distribution. The agglomeration structure due to the dynamic behavior of water molecules containing a hydrogen bonding network is called "water structure".

In the case of biological tissues, biomolecules such as proteins, nucleic acids, and lipids interact with surrounding water and other molecules to form hierarchical structures. In the hierarchical structure, water molecules are also incorporated and structuring, causing slow dynamics. The considerations of slow dynamics with structuring water molecules is a universal concept which is common for the study of liquid structures. Researches on the molecular mechanism of these water structure formations and the manifestation of physical properties and functions are gradually

progressing. However, the interpretation of water structure is still often unclear even in a typical complex dynamics of water molecules, and there exist many phenomena that have not been fully elucidated.

In the recent dielectric spectroscopy analysis of water-mixed systems containing various solute molecules and dispersed particles from polymers to low molecular weight liquids, we have systematically investigated relaxation processes caused by hydrogen bond network dynamics. It was found that the water structure of various water mixing systems reflects the agglomeration structure of solutes and dispersed particles from the characterization by τ–β diagram [6-8] obtained from the relaxation time τ, and the relaxation time distribution parameter β, in the Cole-Cole equation [9]. The fractal concept using τ–β diagrams is extremely broad, allowing universal analysis and discussion of water structures at various scales from the microscopic molecular level to the macroscopic level of material structures including biological tissues [10, 11]. In addition, since dielectric spectroscopy with open-ended coaxial electrodes allows non-invasive measurements, the measurement target regardless of *in vivo* or *in vitro*, and it is possible to discuss uniformly various measuring object.

In this study, the molecular mechanism was elucidated by universal interpretation focusing on various water structures for regarding the physical properties and functions of biological models organized across the hierarchy from the molecular level to the organizational level using microwave dielectric spectroscopy (10 MHz to 65 GHz), and the validity of the physical properties and function evaluation applied to it was discussed.

1.2 Dielectric theory

In this section, the dielectric theory will be described based on the static dielectric constant [12, 13].

In the case of one parallel plate capacitor placed in a vacuum, a charge surface density A charge is stored in the polar plates when a voltage V is applied between the polar plates. The distance between the polar plates is d, the area of the electrode plates is S, and the charges on each polar plate are $-\sigma_0 S$ and $+\sigma_0 S$. The magnitude of the electric field generated by this charge is given as

$$E = \frac{\sigma_0}{\varepsilon_0},$$ (1.1)

where ε_0 is the dielectric constant of a vacuum. The absolute value of the voltage applied across the capacitor to charge $+\sigma S$ is

$$V = |E|d.$$ (1.2)

The centers of positive and negative charges are shifted and dielectric polarization occurs when a dielectric material is inserted between the polar plates. The voltage when a dielectric material is

inserted can be expressed as

$$E = \frac{\sigma}{\varepsilon},$$ (1.3)

where ε is the dielectric constant when a dielectric material is inserted. The relative dielectric constant ε_r, is expressed by the ratio of these dielectric constants as

$$\varepsilon_r = \frac{\varepsilon}{\varepsilon_0},$$ (1.4)

where ε_r is called that dielectric constant.

A polarization charge with a charge surface density $\pm\sigma_P$ opposite to the charge supplied from the power source is generated in the vicinity of the polar plate due to the polarization. The magnitude of the dipole moment due to the polarization charge is $\pm\sigma_P S d$. The magnitude of the dipole moment is proportional to the volume and is equal to σ_P per unit volume. When proportional to the electric field to which polarization is applied, this is expressed as

$$\boldsymbol{P} = \chi\varepsilon_0\boldsymbol{E},$$ (1.5)

and its magnitude is

$$|\boldsymbol{P}| = \sigma_P = \chi\varepsilon_0 E,$$ (1.6)

where χ is the dielectric susceptibility.

A portion of the charge that is canceled by the polarization charge must be supplied to maintain the voltage between the polar plates. The charge surface density stored in the polar plate is expressed as

$$\begin{aligned}
\sigma &= \sigma_0 + \sigma_P \\
&= \varepsilon_0 E + x\varepsilon_0 E \\
&= (1+x)\varepsilon_0 E \\
&= \varepsilon_r\varepsilon_0 E.
\end{aligned}$$ (1.7)

The electric flux density D can be expressed as

$$D = \varepsilon_r\varepsilon_0 E.$$ (1.8)

1.3 Dielectric relaxation phenomenon

Dielectric polarization can be classified into electronic polarization, ionic polarization, and orientation polarization. The time from application of an electric field to the arrival of equilibrium is short in the order of electronic polarization, ionic polarization, and orientation polarization. Orientation polarization occurs when molecules with a permanent dipole moment are oriented in the direction of the electric field. The dynamic properties of the molecules in the dielectric change periodically, therefore, a complex dielectric constant is introduced. A periodic electric field expressed as

$$E(t) = E_0 \cos\omega t,$$ (1.9)

is applied to the dielectric material for a long time. The electrical displacement D, also changes periodically, and the phase changes to show the phase difference ϕ as

$$
\begin{aligned}
D &= D_0 \cos(\omega t - \phi) \\
&= D_1 \cos \omega t + D_2 \sin \omega t,
\end{aligned} \tag{1.10}
$$

however, there are the following conditions:

$$
\begin{aligned}
D_1 &= D_0 \cos \phi, \\
D_2 &= D_0 \sin \phi.
\end{aligned} \tag{1.11}
$$

D_0 is generally proportional to E_0, therefore, it is expressed as

$$
\begin{aligned}
D_1 &= \varepsilon' \varepsilon_0 E_0, \\
D_2 &= \varepsilon'' \varepsilon_0 E_0.
\end{aligned} \tag{1.12}
$$

The formula introduces is expressed as

$$
\varepsilon^* = \varepsilon' - j\varepsilon'', \tag{1.13}
$$

where ε^* is the complex permittivity and j is an imaginary unit. The electric field is rewritten as

$$
\boldsymbol{E} = E(t) = E_0 \exp(-j\omega t), \tag{1.14}
$$

and can be expressed as

$$
\boldsymbol{D} = \varepsilon^* \varepsilon_0 \boldsymbol{E}, \tag{1.15}
$$

which is the same form as the static dielectric constant.

When an electric field $E(u)$ is applied to a dielectric material containing a permanent dipole between time u and $u + du$, it is expressed as

$$
dD(t) = \alpha(t - u)\varepsilon_0 E(u) du, \tag{1.16}
$$

where $\alpha(t-u)$ is a dielectric aftereffect function, which indicates that $dD(t)$ decreases due to relaxation of the orientation polarization. There are components in electrical displacement that can keep up with changes with only a slight time delay. If the term is $\varepsilon_\infty \varepsilon_0 E(u)$, then it is expressed as

$$
dD(t) = \varepsilon_\infty \varepsilon_0 E(u) du + \alpha(0)\varepsilon_0 E(u) du, \tag{1.17}
$$

where it is assumed that α takes a constant value of $\alpha(0)$, while $u < t < u+du$.

An electric field $E(u)$ that starts with $u = 0$ and changes with time is applied to the dielectric material. If the electric displacement $D(t)$ is linear, then it is expressed as

$$
D(t) = \varepsilon_\infty \varepsilon_0 E(t) + \int_0^\infty \alpha(t - u)\varepsilon_0 E(u) du. \tag{1.18}
$$

This can then be expressed as

$$
D(t) = \varepsilon_\infty \varepsilon_0 E(t) + \varepsilon_0 E_0(t) \int_0^\infty \exp(-j\omega t)\alpha(t - u) du, \tag{1.19}
$$

when the electric field is applied for a long time. The complex permittivity is expressed as

$$
\varepsilon^* = \varepsilon_\infty + \int_0^\infty \alpha(x) \exp(-j\omega x) dx, \tag{1.20}
$$

from Eq. (1.15). Assuming the following equation,

4

$$\alpha(x) = \frac{\varepsilon_S - \varepsilon_\infty}{\tau} exp\left(-\frac{x}{t}\right),\tag{1.21}$$

then the following equation

$$\varepsilon^* - \varepsilon_\infty = \frac{\varepsilon_S - \varepsilon_\infty}{\tau} \int_0^\infty exp\left(-j\omega t - \frac{x}{\tau}\right),\tag{1.22}$$

is obtained. Solving this integral gives,

$$\varepsilon^* - \varepsilon_\infty = \frac{\varepsilon_S - \varepsilon_\infty}{1 + j\omega\tau} = \frac{\Delta\varepsilon}{1 + j\omega\tau},\tag{1.23}$$

which is called the Debye equation, where ε_∞ is the high-frequency limit of the dielectric constant, ε_s is the static dielectric constant,$\Delta\varepsilon$ is the relaxation strength, and τ is the relaxation time.

In the case of a relaxation process by orientation polarization of a molecule having an electrode dipole moment, the relaxation time τ is a measure of the speed of molecular motion, and the relaxation strength $\Delta\varepsilon$ is dependent on the magnitude of the dipole moment, the number in a unit volume. Debye's equation can be used to describe experimentally obtained relaxation processes of pure water.

However, any actual dielectric measurement results cannot be well described by Debye's equation. Cole. K. S. and Cole. R. H. expressed the relaxation function as

$$\varepsilon^* - \varepsilon_\infty = \frac{\Delta\varepsilon}{1 + (j\omega\tau)^\beta} \quad (0 < \beta \leq 1)\tag{1.24}$$

which is known as the Cole-Cole equation [9]. β is the relaxation-time distribution parameter. This Cole-Cole equation can well describe a symmetrically spreading relaxation. Though Eq. (1. 24) has been treated as an empirical expression, physical meaning of the shape parameter, β, couldn't been theoretically explained until 1990's, as shown in following section.

1.4 Fractal concept

Fractal structure representation is used to characterize the water structure. In this section, the concept of a fractal is briefly explained.

Consider the case where a similar structure is embedded at a different scale. If a part is taken out and enlarged as much as the whole, then a structure similar to the original structure can be obtained. Alternatively, the overall reduced structure can be considered as a part of the original structure, which is termed self-similarity [14, 15].

Mandelbrot realized early on that many patterns found in nature are self-similar. It has been argued that self-similarity is often hidden, even in featureless random patterns. Mandelbrot proposed a new

concept of fractals and attempted to describe a pattern that showed self-similarity. A pattern with this self-similarity is called a self-similar fractal.

Consider regular self-similar fractals, taking the Koch curve for example, which is very often used when discussing fractals. A Koch curve is a figure obtained by dividing a line segment into three equal parts and indefinitely drawing an equilateral triangle with two divided points as vertices. The length of the Koch curve obtained by repeating the operation indefinitely cannot be defined because the length of the line segment is turn out four-thirds times in one-time operation. Thus, the characteristic of the self-similar fractal is that no characteristic length is found in the pattern. The Koch curve is a continuous but non-differentiable curve.

Quantification of self-similar fractals and expressing them numerically is the quantity called fractal dimension. The fractal dimension is the most important quantity that characterizes self-similar fractals.

1.5 Fractal analysis

The τ–β diagram is obtained from the relaxation time τ and the Cole-Cole parameter that is the relaxation time distribution parameter β obtained from dielectric spectroscopy measurements. The τ–β diagram represents the water structure reflecting the polymer structure and dynamics in the water-mixed system, and the plotted area is divided according to the type and structure of the polymer, such as an aqueous solution system or a gel dispersion system.

Ryabov et al. expressed the relationship between the Cole-Cole parameter β and the relaxation time τ in the fractal structure expression [16]

$$\beta = \frac{d_G}{2} \frac{\ln(\tau \omega_s)}{\ln(\tau/\tau_0)} \tag{1.25}$$

where τ_0 is the cutoff time of the scaling in the time domain, d_G is the fractal dimension of the point set where relaxing units interact with the statistical reservoir,

$$\omega_s = 2 d_E G^{2/d_G} D_s \big/ R_0^2 \tag{1.26}$$

is the characteristic frequency of the self-diffusion process where d_E is the Euclidean dimension, Ds is the self-diffusion coefficient, R_0 is the cutoff size of the scaling in space, and G is a geometrical coefficient approximately equal to unity.

A recent approach using the switching model of hydrogen bonds to explain the molecular mechanism of 10 GHz frequency process of dielectric spectroscopy for alcohols in polymer solutions suggests that the process reflects a rate process of exchanging hydrogen bonds. The collective dynamics of hydrogen bonds exhibit dynamic behaviors of the hydrogen bonding network for various water structures. The fractal analysis suitably characterizes such dynamic networks because of the fractal nature of water structures in complex systems [17].

References

[1] S. Mashimo, N. Miura, and T. Umehara, The Structure of Water and Methanol in p-Dioxane as Determined by Microwave Dielectric Spectroscopy, J. Chem. Phys., 96 (1992) 6358-6361.

[2] U. Kaaze, Complex Permittivity of Water as a Function of Frequency and Temperature, J. Chem. Eng. Data., 34 (1989) 371-374.

[3] R. Buchner, J. Barthel, and J. Stauber, The Dielectric Relaxation of Water between 0°C and 35°C, Chem. Phys. Lett., 306 (1999) 57-63.

[4] T. Fukasawa, T. sato, J. Watanabe, Y. Hama, W. Kunz, and R. Buchner, Relation between Dielectric and Low-Frequency Raman Spectra of Hydrogen-Bond Liquids, Phys. Rev. Lett., 95 (2005) 1-4.

[5] S. Schrodle, G. Hefter, and R. Buchner, Dielectric spectroscopy of hydrogen bond dynamics and microheterogenity of water-dioxane mixtures, J. Phys. Chem., 111 (2007) 5946-5955.

[6] Y. E. Ryabov, Y. Feldman, N. Shinyashiki, and S. Yagihara, The symmetric broadening og the water relaxation peak in polymer-water mixtures and its relaxationship to the hydrophilic and hydrophobic properties of polymers, J. Chem. Phys., 19 (2002) 8610-8615.

[7] Y. E. Ryabov, and Y. Feldman, The Relationship between the scaling parameter and relaxation time for non-exponential relaxation in disordered systems, Fractals., 11 (2003) 173-183.

[8] N. Shinyashiki, S. Yagihara, I. Arita, and S. Mashimo, Dynamics of Water in a Polymer Matrix Studied by a Microwave Dielectric Measurement, J. Phys. Chem. B 102 (17), 3249-3251 (1998)

[9] K. S. Cole, and R. H. Cole, Dispersion and Absorption in Dielectrics, J. Chem. Phys., 9 (1941) 341-351.

[10] S. Yagihara and N. Shinyashiki, Dynamics of water Structure in Biological System and Broadband Dielectric Spectroscopy, SEIBUTSU BUUTSURI (Japanese), 44 (2004) 4-9.

[11] S. Yagihara, Fundamental Study and Application of Water Structures in Foods and Related Materials by Broadband Dielectric Spectroscopy (BDS), Nestle Science Promotion Committee Annual Report, (2005) 89-99

[12] H. Frolish, Theory of dielectrics: dielectric constant and dielectric loss (Japanese, K. Nagamiya and Y. Nakai Trans.), (1963) Yoshioka Shoten.

[13] Y. Hayashi, Department of Physics, Graduate School of Science, Tokai University, (2001) Doctoral thesis.

[14] M. Matsusita, Fractal physics[Translated from Japanese], (2002) Shokabou.

[15] J.Feder, Fractal (M. Matsushita, Y. Hayakawa and S. Sato trans.), (1991) Tetsugaku Shuppan.

[16] Y. E. Ryabov, Y. Feldman: Fractals 11 (2003), 173-183.

[17] S. Yagihara, R. Kita, N. Shinyashiki, H. Saito, Y. Maruyama, T. Kawaguchi, K. Shoji, T. Saito, T. Aoyama, K. Shimazaki, K. Matsumoto, M. Fukuzaki, H. Masuda, S. Hiraiwa, K. Asami and

M. Tokita, Physical Meanings of Fractal Behaviors of Water in Aqueous and Biological Systems with Open-Ended Coaxial Electrode, Sensors, 19 (2019).

Chapter 2

Experimental methods

Experimental techniques for dielectric and nuclear magnetic resonance measurements have been developed especially for water structure analysis by our research group. These techniques have already been reported in various scientific journals and in reports on various research projects. In this chapter, an outline and some details of original techniques with measuring systems are described.

2.1 Dielectric spectroscopy

Polarization P occurs when an electric field is applied to a dielectric material. P is expressed as

$$D = \varepsilon_r \varepsilon_0 E = \varepsilon_0 E + P, \tag{2.1}$$

from the relationship between the electric flux density D and the electric field E, where ε_0 is the dielectric constant in a vacuum, ε_r is the relative dielectric constant, and ε_r is expressed as

$$\varepsilon_r = \varepsilon / \varepsilon_0, \tag{2.2}$$

where ε is the dielectric constant of the dielectric material. The relative permittivity ε_r in an AC electric field is defined as the complex permittivity ε^* as follows

$$\varepsilon^* = \varepsilon' - j\varepsilon'', \tag{2.3}$$

where j is an imaginary number, and ε' and ε'' are defined as the dielectric constant and dielectric loss, respectively.

2.1.1 Time Domain Reflectometry (TDR) method

The Time Domain Reflectometry (TDR) method [1-4] is a technique used to measure the complex dielectric constant in the frequency range from 100 MHz to 65 GHz. A reflected signal that includes information on the dielectric constant of the sample is observed when a step pulse is incident on the sample. The frequency dependence of the complex dielectric constant can be obtained by measuring the reflected signal in the time domain and performing a Fourier transform.

Direct method

The complex permittivity of the sample can be expressed by the basic equation of the TDR method as

$$\varepsilon^* = \frac{c'}{j\omega\gamma d} \frac{v_0 - r}{v_0 + r} X \cot X, \tag{2.4}$$

where c' is the speed of propagation in the coaxial line, v_0 and r are the Laplace transforms of the incident and reflected pulse waveforms, respectively, X is $(\omega d/c)\varepsilon^{*1/2}$, $X \cot X$ takes into account propagation and multiple reflections in the sample and the coaxial-line geometry, and γd is an electric length. This equation shows that the complex permittivity of the sample can be obtained from measurements of the incident and reflected pulses.

Reference method

The reference method uses the difference between the reflected signal from a standard sample with a known complex dielectric constant and the reflected signal from an unknown sample. Water, acetone, methanol, and dimethyl sulfoxide (DMSO), and so on with known complex dielectric constants are used as standard samples. The reference method is more accurate than the direct method.

The basic equation of the direct method is expressed as

$$
\begin{cases}
\varepsilon_{s*} = \dfrac{c'}{j\omega\gamma d} \dfrac{v_{0(\omega)} - r_{s(\omega)}}{v_{0(\omega)} + r_{s(\omega)}} X_s \cot X_s \\[4mm]
\varepsilon_{x*} = \dfrac{c'}{j\omega\gamma d} \dfrac{v_{0(\omega)} - r_{x(\omega)}}{v_{0(\omega)} + r_{x(\omega)}} X_x \cot X_x
\end{cases}
\tag{2.5}
$$

where the complex permittivity of the standard sample is defined as $\varepsilon_s{}^*$ and the complex permittivity of the unknown sample is defined as $\varepsilon_x{}^*$. For these equations, when the incident wave $v_0(\omega)$ is eliminated and $\varepsilon_x{}^*$ is solved, it is expressed as

$$
\varepsilon_{x*} = \varepsilon_s * \frac{1 + \rho \dfrac{c' f_s}{j\omega\gamma d \varepsilon_s *} f_s}{1 + \rho \dfrac{j\omega\gamma d \varepsilon_s *}{c' f_s} f_x}
\tag{2.6}
$$

$$
\begin{cases}
\rho = \dfrac{r_s(\omega) - r_x(\omega)}{r_s(\omega) + r_x(\omega)} \\[4mm]
f_s = X_s \cot X_s, \; X_s = \dfrac{\omega d \sqrt{\varepsilon_s *}}{c} \\[4mm]
f_x = X_x \cot X_x, \; X_x = \dfrac{\omega d \sqrt{\varepsilon_x *}}{c}
\end{cases}
\tag{2.7}
$$

This equation is the basic equation of the TDR method by the reference method.

2.2 Impedance measurement method

The capacitance changes to a value that reflects the dielectric constant of a dielectric material when it is inserted into a capacitor having a known capacitance. A capacitor with a dielectric material

inserted can be considered equivalent to an RC parallel circuit. Therefore, the complex permittivity specific to a substance can be obtained from the capacitance component Cp and resistance component Rp of this equivalent circuit [5, 6].

The admittance for a capacitor when a dielectric material is inserted is expressed as

$$Y = j\omega C,$$ (2.8)

where C is the capacitance. When the capacitance C_0 of a known capacitor changes depending on the complex permittivity of the dielectric material, it can be expressed as

$$\begin{aligned} Y &= j\omega C \\ &= j\omega C_0 \varepsilon^* \\ &= \omega C_0 \varepsilon'' + j\omega C_0 \varepsilon'. \end{aligned}$$ (2.9)

This is equivalent to an RC circuit, therefore, the admittance can also be expressed as

$$Y = \frac{1}{R_p} + j\omega C_p.$$ (2.10)

The complex permittivity can be derived from Eqs. (2.9) and (2.10) as

$$\varepsilon' = \frac{C_p}{C_0},$$ (2.11)

$$\varepsilon'' = \frac{1}{\omega C_0 R_p}.$$ (2.12)

2.3 Frequency sweep dielectric measurement method

The signal source sends a single frequency signal to the material. The receiver is tuned to that frequency to detect the reflected and transmitted signal from the material. The amplitude and phase data of that frequency can be obtained from the measured response. The signal source is changed to the next frequency, the measurement is repeated, and the reflection and transmission response is obtained as a function of frequency. The complex dielectric constant $\varepsilon^*(\omega)$ is obtained following the procedure reported by Bao et al. [7] from the complex reflection coefficient $\Gamma^*(\omega)$, through the relationship

$$\varepsilon^*(\omega) = \frac{A_1^*(\omega)\Gamma^*(\omega) - A_2^*(\omega)}{A_3^*(\omega) - \Gamma^*(\omega)},$$ (2.13)

where $Aj(\omega)$ ($j = 1, 2, 3$) are frequency-dependent complex constants that can be obtained from a calibration procedure performed with air, short connections, and water [8].

2.4 Pulse Field Gradient - Spin Echo method of Nuclear Magnetic Resonance (PGSE-NMR)

In the Pulse Field Gradient - Spin Echo method [9, 10], spatial anisotropy is applied by a gradient magnetic field, and the diffusion coefficient D is measured from the disorder of the phase of the magnetic dipole. The self-diffusion of molecules is calculated from the echo signal attenuation. In the spectrum decay process when the gradient magnetic field is changed with respect to the sample, the echo signal intensity is A, the spectrum intensity obtained with the first gradient magnetic field is $A(0)$, and the spectrum intensity after that is $A(\delta)$, These ratios are expressed by Stejskal-Tanner's formula

$$\ln\left[\frac{A(\delta)}{A(0)}\right] = -\gamma^2\delta^2 g^2 D\left(\Delta - \frac{\delta}{3}\right), \tag{2.14}$$

where γ is the gyromagnetic ratio, g is the magnetic field gradient, δ is the field gradient pulse duration, and Δ is the separation of gradient pulses.

References

[1] K. S. Cole, and R. H. Cole, Dispersion and Absorption in Dielectrics, J. Chem. Phys., 9 (1941) 341-351.

[2] R. H. Cole, Evaluation of Dielectric Behavior by Time Domain Spectroscopy. I. Dielectric Response by Real Time Analysis, J. Phys. Chem., 79 (1975) 1459-1469.

[3] R. H. Cole, Evaluation of Dielectric Behavior by Time Domain Spectroscopy. II. Complex Permittivity, J. Phys. Chem., 79 (1975) 1469-1474.

[4] R. H. Cole, S. Mashimo, and P.Winsor IV, Evaluation of Dielectric Behavior by Time Domain Spectroscopy. 3. Precision Difference Methods, J. Phys. Chem., 84 (1980) 786-793.

[5] Agilent Technologies, "Impedance measurement handbook" [Translated from Japanese.], (http://literature.cdn.keysight.com/litweb/pdf/5950-3000JA.pdf).

[6] Keysight Technologies, "Impedance measurement basics" [Translated from Japanese.], (https://www.keysight.com/upload/cmc upload/All/impedance for web seminar.pdf).

[7] J. Z. Bao, C. C. Davis, and M. L. Swicord, Microwave Dielectric Measurements of Erythrocyte Suspensions, Biophys. J., 66 (1994) 2173–2180.

[8] C. Cametti, S. Marchetti, C.M.C. Gambi, and G. Onori, Dielectric relaxation spectroscopy of lysozyme aqueous solutions analysis of the δ-dispersion and the contribution of the hydration water, J. Phys. Chem., 115 (2011)7144-7153.

[9] Farrar, T.C., Becker, E.D., "Pulse and Fourier Transform NMR", Academic Press, New York (1971)

[10] E. O. Stejskal, and J. E. Tanner, Spin Diffusion Measurements: Spin Echoes in the Presence of a Time-Dependent, J. Chem. Phys., 42 (1965) 288-292.

Chapter 3

Complementary Analyses of Fractal and Dynamic Water Structures in Protein-Water Mixtures and Cheeses

3.1 Introduction

Water is a typical hydrogen-bonding liquid consisting of molecules having hydroxyl groups with both donor and acceptor site of hydrogen bonding. Water molecules exhibit Brownian movements, repeating breakup and recombination of hydrogen bonds. The breakup and recombination are considered as elementary processes of intermolecular correlations in the liquid structure, and interpret a model in which a concept of the dynamic cluster formed by 5-6 water molecules is often used today [1]. Generation and annihilation of such dynamic clusters of water molecules observed as a single relaxation process of Debye type by dielectric spectroscopy suggests why specific behaviors of the water are shown. The relaxation process observed for water indicates that the relaxation time τ is 8.27ps at 25°C [2-5]. The relaxation time is a characteristic time of rotational diffusion of molecules, while the presence of a small relaxation process reflecting more local dynamics has been reported in one or more decades higher frequency range of THz region. The elementary process of break up and recombination of hydrogen bonding may be closely related to this THz frequency process, the detailed discussion has not been completed yet.

A dynamic agglomeration structure of water molecules interacting with surrounding molecules identified by those dynamics behaviors is called water structure. In recent years, molecular mechanisms forming water structures has been extensively investigated in various polymer-water mixtures, and an importance to incorporate the handling of hydrogen bond network is pointed out in the interpretation of water structures. However, the dynamic range of molecular behaviors of water is extremely wide under various conditions, and those understanding have been delayed due to the dearth of enough wide time scale in conventional observation techniques. Then complementary experimental techniques of molecular dynamics in different time scales must be effective to discuss water structures in a wide time scale. The interpretation thus focused on the dynamic behavior of water molecules should be effectively employed in extensive area of applications as well as fundamental researches [6].

The relaxation time obtained for the relaxation process due to molecular dynamics of water increases and the distribution is broadened with increasing concentration in polymer-water mixtures. This behavior is called slow dynamics, and is an important concept to explain liquid structures,

polymers, proteins, nucleic acids, and lipid molecules in biological systems, in which hierarchical structures of water molecules with solute molecules and dispersed particles appear. In order to characterize these hierarchical structures, fractal concept should be helpful because of the multi scaled treatment [7, 8]. It is reasonably expected that the fractal concept can be utility to characterize various water structures.

The fractal expression of the relaxation process for water molecules obtained by dielectric spectroscopy has been developed to apply to various aqueous systems [9, 10]. When exponential hyperbolic type dipolar correlation function corresponding to Cole-Cole equation [11] was compared with memory function, it was shown that exponent of Cole-Cole type and spatial-temporal fractal dimension are well corresponding. Cole-Cole equation is expressed as

$$\varepsilon^* - \varepsilon_\infty = \frac{\Delta\varepsilon}{1+(j\omega\tau)^\beta} \quad (0 < \beta \leq 1) \tag{3.1}$$

where ε^* is the complex dielectric permittivity, ε_∞ is the high frequency limit of the dielectric constant, $\Delta\varepsilon$ is the relaxation strength, j is the imaginary unit, ω is the angular frequency, τ is the relaxation time, and β is the relaxation time distribution parameter. The space fractal dimension to scale the volume division size of the relaxation structure unit is obtained from Eq. (3.1) with a relationship between, the relaxation time, and the exponential of Cole-Cole type relaxation time distribution through relaxation processes dependent on the water content.

In this study, we performed TDR measurements on protein-water mixtures and cheeses in order to investigate water structures. NMR measurements on diffusion process of water molecules are also performed to compare the results with the relaxation parameter obtained from TDR measurements. It is expected that molecular dynamics related with the rotational and the translational diffusion, respectively, by TDR and NMR measurements with different characteristic time scales of observation are compared. Fractal analysis using the τ–β diagram obtained from TDR measurements is also examined to discuss hierarchical structures of water and proteins. We focus on the space fractal dimension as physical quantity to characterize water structures of water mixtures.

3.2 Experimental

3.2.1. Sample Preparations

Albumin from bovine serum (BSA), Ovalbumin (OVA), and Lysozyme from Chicken Egg-White (CEWL) were purchased from Sigma-Aldrich. Each protein was mixed with distilled water (Millipore, ultrapure water with resistivity higher than 18.2 MΩ・cm). Each protein concentration was adjusted to 5, 10, 20, 30, and 40 wt%.

Various kinds of cheese available in market were purchased. Prepared in the present work were mozzarella cheese (KRAFT), camembert cheese (MEGMILK SNOW BRAND Co.,Ltd.), cream

cheese (Bel Japon K.K.), processed cheese (MEGMILK SNOW BRAND Co.,Ltd.), gouda cheese (TOKYO DAIRY CO.,LTD), and red cheddar cheese (TOKYO DAIRY CO.,LTD).

Samples were kept in the refrigerator before measurements, and the sample temperature was kept at 25.0±0.2 °C during both TDR and NMR measurements.

3.2.2 Time Domain Reflectometry Measurements and Fractal Analysis

Digitizing Oscilloscope Mainframe (HP 54120B) and its Four Channel Test Set (HP 54124A) was employed as the TDR system [12-16] to make dielectric measurements especially for a relaxation process due to molecular dynamics of free water in the frequency range from 0.1 to 30 GHz. Reflected signal including information of the dielectric behavior of the sample responding to the incident step pulse was observed.

The complex permittivity of the sample can be expressed by the basic equation of TDR method [12-14] as

$$\varepsilon_* = \frac{c'}{j\omega\gamma d}\frac{v_0 - r}{v_0 + r}X\cot X \tag{3.2}$$

where c' is the speed of propagation in a coaxial line, v_0 and r are the Laplace transforms of the incident and reflected pulse waveforms, $X\cot X$ is propagation and multiple reflections in the sample and coaxial line geometry, and γd is a value of corrective coefficient. Since accuracy would be better off using the difference method [12-14].

50Ω semi-rigid coaxial cable (SUHNER) with outer diameter d = 2.2 mm and electric length γd = 0.165 mm is used for electrodes of the TDR measurement.

The τ–β diagram shows the characteristic behavior of slow dynamics for each material, and some tendencies were obtained for the type of polymers.

Ryabov et al. expressed the relationship between the Cole-Cole parameter β and the relaxation time τ in the fractal structure expression[9]

$$\beta = \frac{d_G}{2}\frac{\ln(\tau\omega_s)}{\ln(\tau/\tau_0)} \tag{3.3}$$

where τ_0 is the cutoff time of the scaling in time domain, d_G is the fractal dimension of the point set where relaxing units are interacting with the statistical reservoir,

$$\omega_s = 2d_E G^{2/d_G}D_s\big/R_0^2 \tag{3.4}$$

is the characteristic frequency of the self-diffusion process where d_E is the Eucidean dimension, Ds is the self-diffusion coefficient, R_0 is the cutoff size of the scaling in the space, and G is a geometrical coefficient approximately equal to unity.

3.2.3 Frequency Sweep Dielectric Measurements

Frequency sweep dielectric measurements were carried out using a Vector Network Analyzer (Agilent N5230C) with a dielectric kit probe (Agilent 85070E) in the frequency range from 0.5 to 50 GHz.

VNA measurements offers the complex reflection coefficient $\Gamma^*(\omega)$, from which the complex dielectric constant $\varepsilon^*(\omega)$ is obtained following the procedure reported by Bao et al.[17], through the relationship

$$\varepsilon^*(\omega) = \frac{A_1^*(\omega)\Gamma^*(\omega) - A_2^*(\omega)}{A_3^*(\omega) - \Gamma^*(\omega)} \tag{3.5}$$

where $A_j(\omega)$ (j = 1,2,3) are frequency-dependent complex constants which can be obtained from calibration procedure performed with air, short connections, and water[18].

3.2.4 Pulse-Field Gradient Spin-Echo Method of Nuclear Magnetic Resonance

Nuclear magnetic resonance (NMR) measurements were performed by ^{1}H 90 MHz, FT-NMR, JNM-EX90 (JEOL) for water proton translational diffusion coefficient. Pulse-Field Gradient Spin-Echo (PGSE) method of NMR was used to obtain the diffusion coefficient of water molecules with the gradient field applied parallel to z-axis of rectangle shape of length δ in a Spin-Echo pulse sequence.

In this method, we obtained echo signal at a number of different gradient pulse length, δ. The self-diffusion of molecules is calculated from the echo signal attenuation [19]. The echo amplitude is given by following equation [20],

$$\ln\left[\frac{A(\delta)}{A(0)}\right] = -\gamma^2\delta^2g^2D(\Delta - \frac{\delta}{3}) \tag{3.6}$$

where A is the echo signal intensity, γ is the gyromagnetic ratio, g is the magnetic field gradient, δ is the field gradient pulse duration, and Δ is the separation of gradient pulses.

3.3 Results and discussion

Typical dielectric relaxation spectra obtained by TDR measurements for protein-water mixtures with various concentrations are shown in Fig. 1, where the real part ε' and imaginary part ε'' of the complex permittivity are plotted as a function of frequency f. The relaxation process observed around 10 GHz is considered to be due to rotational diffusion process of water molecules from the relaxation time and the strength. The lower frequency processes reflecting ion behaviors, chain

dynamics, and restricted water molecules are also usually shown for aqueous systems in lower frequency region below 1GHz. The lower frequency processes are larger for CEWL than those for BSA, because the ion concentration is probably larger. Fig.1 shows that dielectric constant is smaller with increasing protein concentration because of decreasing water content. Fig.2 shows the concentration dependence of the relaxation parameters obtained from fitting procedures of Eq. (3.1) to experimental data shown in Fig.1. The relaxation time τ increased and the relaxation-time distribution parameter β and the relaxation strength $\Delta\varepsilon$ decreased with increasing protein concentration. Since $\Delta\varepsilon$ means a magnitude of orientation polarization by dipole moments of water molecules, the decrease in the relaxation strength accompanied by the increase in protein concentration reflects decreasing number density of water molecules in the mixtures. The decrease in β reflecting broadening relaxation curves evaluates the relaxation time distribution, which is corresponding to increasing fluctuation of the dynamics of water molecules caused by larger interactions with protein molecules. The increase in τ shows that the mobility of water molecules decreases by increasing in between polymer chains and water molecules. In these behaviors, the relaxation time is given as a characteristic time of the dynamics of water molecules on the average.

Fig.3 shows the concentration dependence of the diffusion coefficient of water molecules obtained from PGSE-NMR measurements for protein aqueous solution. The diffusion coefficient of pure water is 2.32×10^{-5}/cm^{2}s^{-1}. The diffusion coefficient decreases, as protein concentration becomes higher. This tendency of concentration dependence is corresponding to that obtained for the relaxation time of dielectric spectroscopy. In the relaxation profile obtained by TDR, the rotational diffusion process of water molecules and the distribution are ranging in time scale of picosecond order. On the other hand, the diffusion coefficient of the translational motion obtained by NMR measurement is ranging in millisecond time scale. Then it is suggested that both of rotational and translational diffusion processes are similarly restricted by increasing concentration, and the restriction also affects the mobility in the same manner in picosecond and millisecond time scales.

Dielectric relaxation spectra observed by VNA measurements for various kinds of cheeses are shown in Fig.4. The lower frequency processes are smaller than those observed in protein solutions. It is reasonable to consider that the ion mobility should be smaller in cheese than solutions. The relaxation parameters for the GHz frequency processes were obtained by the same procedures with the case of protein solutions, and are listed in Table 1.

Since there exist some difficulties in evaluation of exact water content of cheese because of the existence of water molecules which cannot be easily removed by usual procedure, the water content is represented by the relaxation strength in the present work. The relaxation strength dependence of the diffusion coefficient of water molecules for cheeses is shown in Fig.5. The diffusion coefficient tends to decrease with decreasing $\Delta\varepsilon$ as shown in Fig.3 for protein solutions. The plot for camembert cheese is shown in the smaller side of the tendency. This deviation should be attributed to the

heterogeneity of hydration.

Generally, aqueous systems show varieties in concentration dependences of relaxation parameters, and it is difficult to find out any universal explanations of water structures. The $\tau-\beta$ diagram created as a relaxation between the average characteristic time and its distribution of water structures is a possible tool as a universal treatment. In our former reports, we indicated that solution systems and dispersed systems were classified and characterized by the locus plotted in the $\tau-\beta$ diagram [21, 22, 23]. Plots of the dispersion systems were shown in the diagram as extended lengthwise forms, and the value of the fractal dimension of the dispersion systems was smaller than 1.0. Any conventional techniques to classify solutions and dispersed systems with a common criterion have not been shown so far.

Fig.6 is $\tau-\beta$ diagram for protein solutions and cheeses. Plots for the present samples were shown in the diagram as extended lengthwise forms, and they are in the area for dispersion systems in Fig.6. Table 2 shows the space fractal dimension, the characteristic frequency of the self-diffusion process, and cutoff time that were obtained by the least-square fit method of Eq. (3.3) with experimental data according the plot of the $\tau-\beta$ diagram. The values of the fractal dimension thus obtained were 0.03 ± 2.45 for BSA, 0.03 ± 1.70 for CEWL, and 0.22 ± 0.89 for OVA. These values are much smaller from those obtained for usual aqueous solution systems, and the error is much larger than usual solutions. Usual values of the fractal dimension obtained for water structures in aqueous polymer solutions are about 1.3-1.5, and error is 0.02-0.71. Water structures with the small fractal dimension give only small increase in the relaxation time with increasing concentration. Then, in order to determine the fractal dimension from the $\tau-\beta$ diagram, a sufficient high-concentration domain is necessarily required. However, it is fairly difficult to prepare high-concentration samples especially for dispersion systems, and the global image of trajectory of the plots cannot be obtained. Therefore the magnitude of error and the fractal dimension are correlated each other, and it is unavoidable to have a large error of the fractal dimension from the geometric condition for dispersion systems [24].

It turns out that physical sense of one or less value of the fractal dimension is proceeding agglomeration in dispersed system from knowledge of our geometric model calculation. The value of such a small fractal dimension is not unreal for dispersed system, and it is strongly dependent on the spatiotemporal scale of analyzing method [25]. The process of the slow dynamics reflects the conformation of polymer chains and those agglomeration structures, and also hydrogen bonding ability. Therefore, characterization of the slow dynamics is not determined only by the absolute value of fractal dimension but also by the geometric feature of the domain where the locus of a plot appears in the $\tau-\beta$ diagram. In the eyes of slow dynamics of water structures shown in the $\tau-\beta$ diagram, protein solutions and cheeses have quite similar water structures with the characteristics of dispersed systems.

The variations of plots obtained for the various kinds of cheese are also shown in Fig.6. Even with

the difference in different kinds of cheese, all plots for cheeses show the water structures of typical dispersion systems. Fig.7 shows plot of the relaxation-time distribution parameter against the inverse of the diffusion coefficient for various cheeses. Figs. 7 and 6 are resembled, and $1/D$-β plot might be also a candidate of a effective tool to characterize water structure. The Stokes-Einstein equation is described with the diffusion coefficient as

$$D = \frac{k_B T}{6\pi\eta R_h} \tag{3.7}$$

where k_B is Boltzmann's constant, T is the absolute temperature, η is viscosity of surrounding medium and R_h is hydrodynamic radius of the motional unit. The Debye-Stokes-Einstein equation is described with the relaxation time as

$$\tau_{rot} = \frac{V\eta}{k_B T} \tag{3.8}$$

where V is volume of the motional unit. Then the relaxation time corresponding to the inverse of the diffusion coefficient suggested by Eq. (3.7) and Eq. (3.8) support the accordance of Figs. 6 and7.

Figs. 8 and 9 show the relaxation strength dependence of the relaxation time and its distribution parameter for cheese. The relaxation strength reflects the water content as expressed by equation as

$$C = \rho_w \frac{\Delta\varepsilon}{\Delta\varepsilon_w} \tag{3.9}$$

where ρ_w and $\Delta\varepsilon_w$ are the density and the relaxation strength of pure water, respectively [23]. Considering that the relaxation strength is proportional to the water content, Figs. 8 and 9 can be treated as usual concentration dependence of physical quantities shown inFig.2. Figs. 8 and 9 show the deviation of the plot for camembert cheese because of the heterogeneous hydration as shown in Fig.5.

The relaxation strength dependence of the relaxation time and its distribution parameter are also shown in Figs. 10 and 11 for protein aqueous solutions. These results indicate the similar tendency with Fig. 2. It is reasonable to consider that water structures interacting with protein structures included in cheese and protein solutions are not necessarily same, since the protein structures, denaturalization, and various additives affect water structures. Actually in the fractal analysis, the τ–β diagram shows different water structures with different values of fractal dimension, however, the water structures in various kinds of cheese and protein solutions are clearly classified in dispersion systems. Fractal analysis with the τ–β diagram using geometric characteristics of the whole diagram can be an effective tool to characterize various water structures.

3.4 Conclusion

It was found that the relaxation profile obtained from TDR measurements indicated that restricted water structures show typical slow dynamics in the picoseconds time scale. The slow dynamics observed for the diffusion process of water molecules observed by PGSE-NMR in millisecond time

scale also shown the similar behavior, even if those physical quantities and the time scales of respective observation techniques were considerably different. Fractal analysis of protein solutions by TDR measurements suggested that water structures in both systems were same with usual dispersion systems much more than solution systems. The fractal analysis with the τ–β diagram using geometric characteristics of the whole diagram is effective to characterize various water structures.
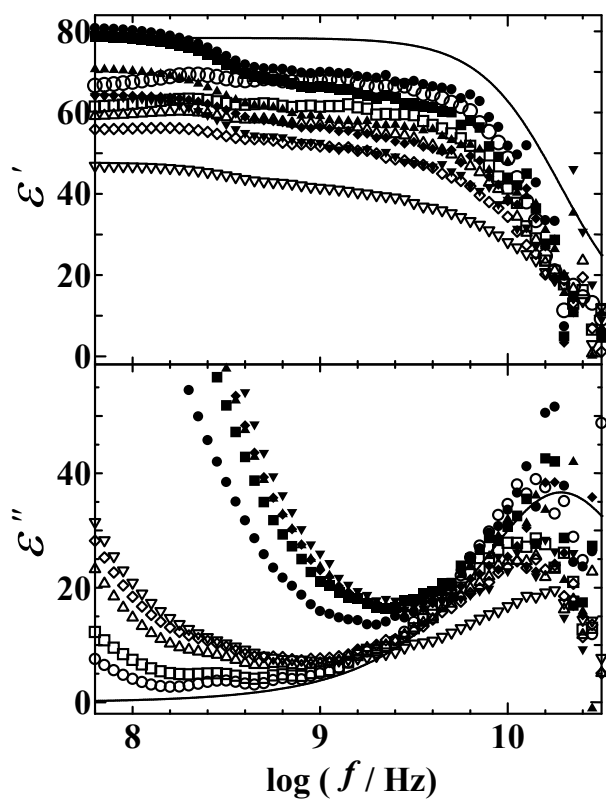
Fig. 1. Frequency dependence of dielectric constant and loss for 5($\bigcirc$), 10($\square$), 20($\triangle$), 30($\diamondsuit$), and 40wt%($\triangledown$) BSA and 5($\bullet$), 10($\blacksquare$), 20($\blacktriangle$), 30($\blacklozenge$), and 40wt%($\blacktriangledown$) CEWL aqueous solutions at 25°C.

[1×10⁻¹²]
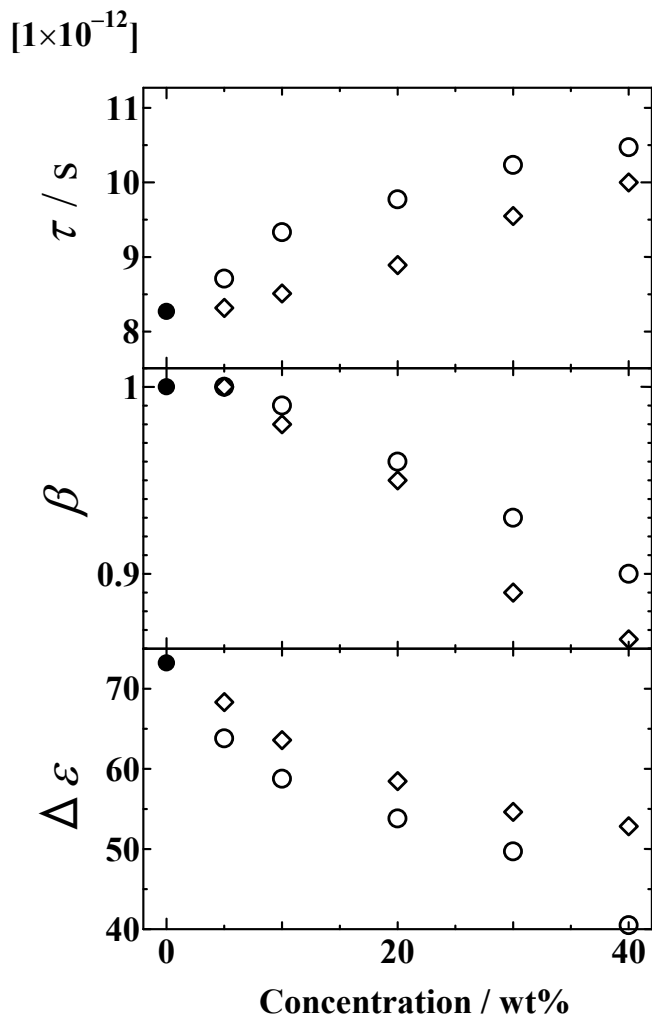
Fig. 2. Concentration dependence of the relaxation strength $\Delta\varepsilon$, the relaxation time τ and the relaxation time distribution parameter $\square$ for BSA(○) and CEWL(◇) aqueous solutions at 25°C.
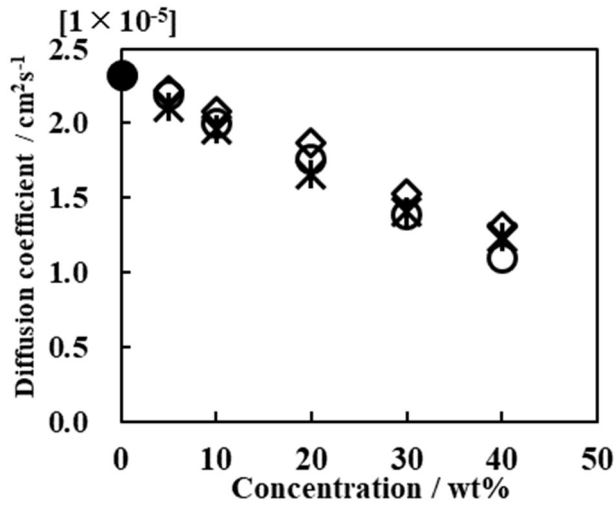
Fig. 3. Concentration dependence of the diffusion coefficient for BSA(○), CEWL(◇) and OVA(＊) aqueous solutions at 25°C.
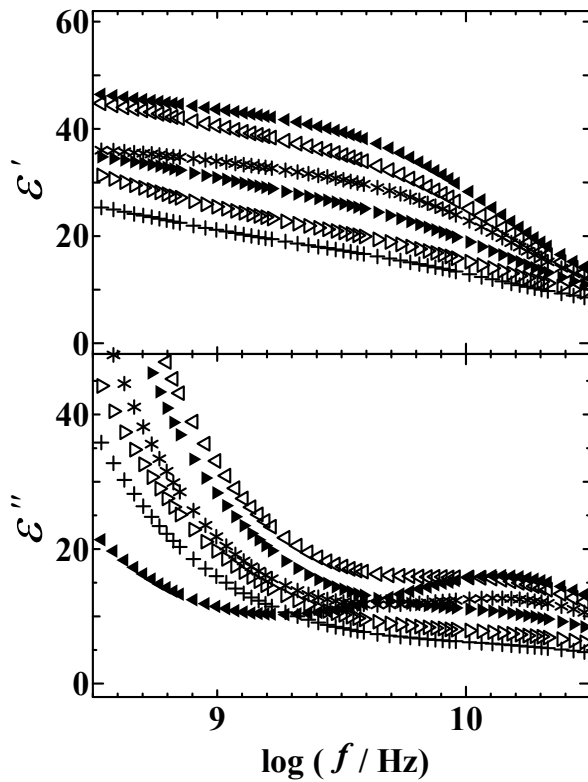
Fig. 4. Frequency dependence of dielectric constant and loss for various kinds of cheeses(mozzarella[◀], camembert[◁], cream[＊], processed[▶], gouda[▷], and red cheddar[＋]).
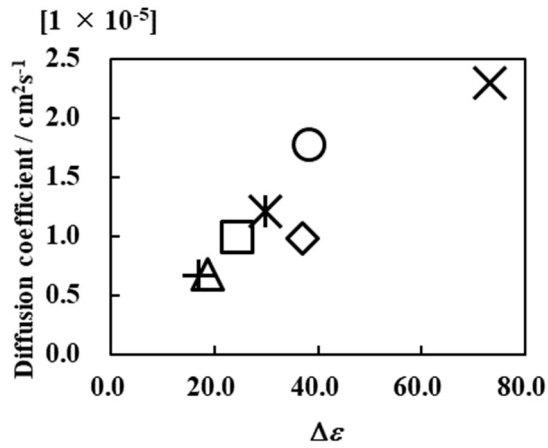
Fig. 5. Plots of the relaxation strength versus the diffusion coefficient for water(×), mozzarella(○), camembert(◇), cream(＊), processed(□), gouda(△), and red cheddar(＋).
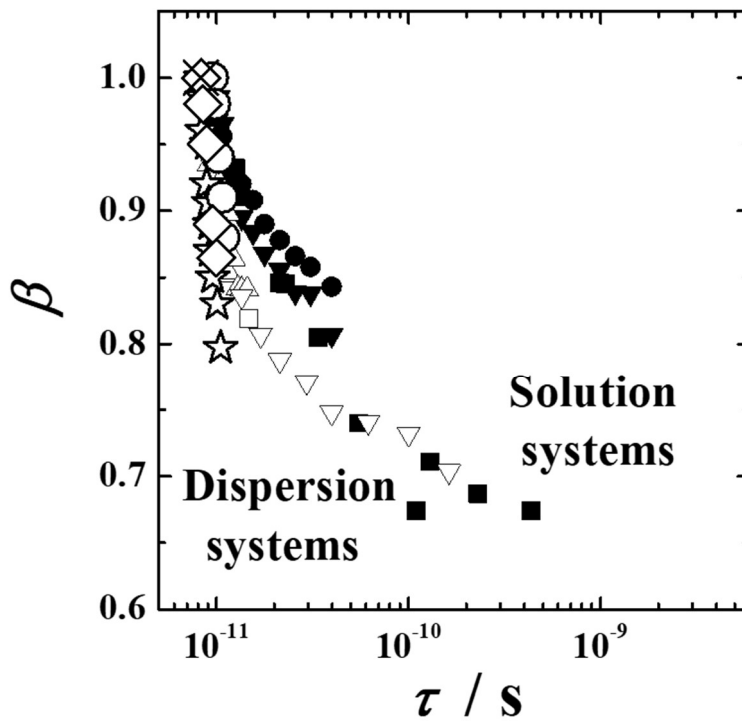
Fig. 6. Diagram of the relaxation time versus the relaxation-time distribution parameter of Cole-Cole equation for water(×), BSA(○), CEWL(◇), OVA(☆), PEG(●), PVP(■), PVME(▼), PVA(△), PAIA(□), and PEI(▽). The inset is the □□□ diagram for proteins(★) and cheeses(mozzarella[◀], camembert[◁], cream[＊], processed[▶], gouda[▷], and red cheddar[＋]).
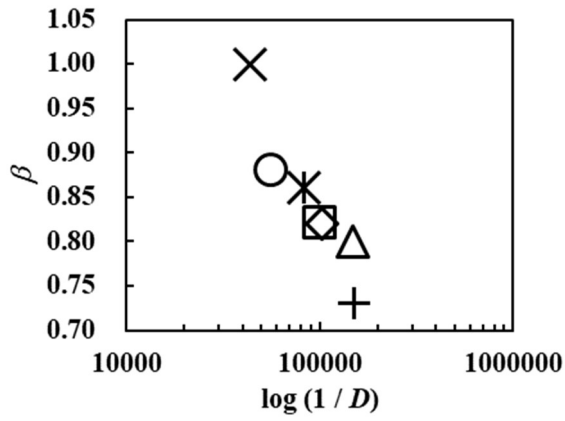
Fig. 7. Plots of inverse of the diffusion coefficient versus the relaxation-time distribution parameter of Cole-Cole equation for water($\times$), mozzarella($\bigcirc$), camembert($\diamondsuit$), cream($*$), processed($\square$), gouda($\triangle$), and red cheddar($+$).
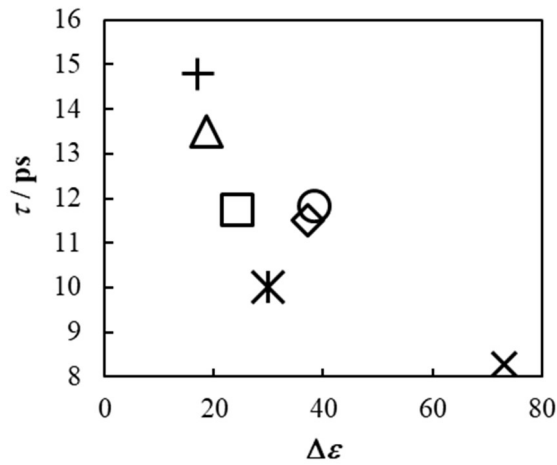
Fig. 8. Plots of the relaxation strength versus the relaxation time for water($\times$), mozzarella($\bigcirc$), camembert($\diamondsuit$), cream($*$), processed($\square$), gouda($\triangle$), and red cheddar($+$).
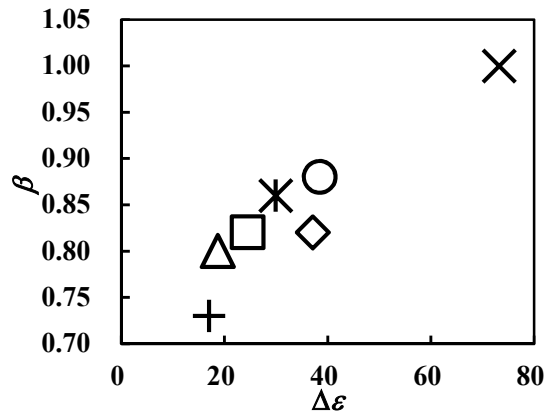
Fig. 9. Plots of the relaxation strength versus the relaxation-time distribution parameter for water($\times$), mozzarella($\bigcirc$), camembert($\diamondsuit$), cream($\ast$), processed($\square$), gouda($\triangle$), and red cheddar($+$).
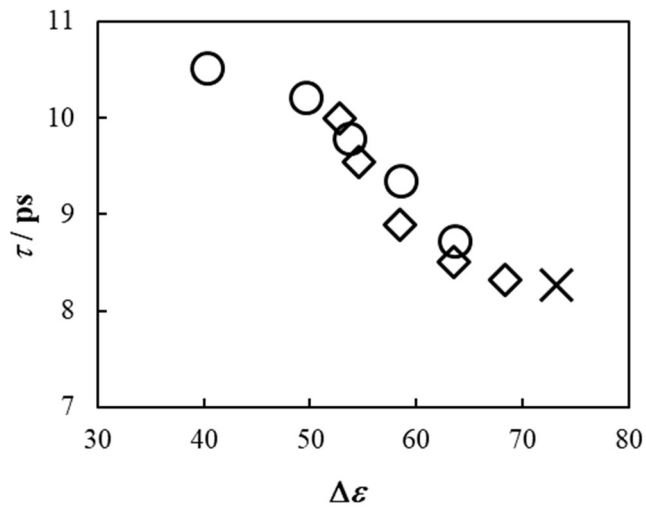
Fig. 10. Plots of the relaxation strength versus the relaxation time for water($\times$), BSA($\bigcirc$), and CEWL($\diamondsuit$) aqueous solutions.
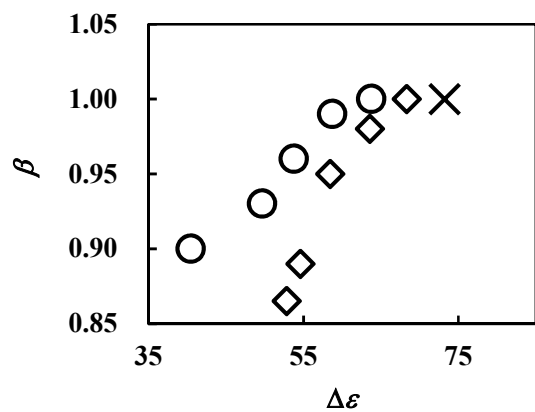
Fig. 11. Plots of the relaxation strength versus the relaxation-time distribution parameter for water($\times$), BSA($\bigcirc$), and CEWL($\diamondsuit$) aqueous solutions.

Table1. Relaxation parameters for water and various kinds of cheeses.

sample	$\Delta\varepsilon$	τ / ps	β
mozzarella cheese	38.5	11.8	0.88
camembert cheese	37.1	11.5	0.82
cream cheese	29.9	10.0	0.86
processed cheese	24.5	11.8	0.82
gouda cheese	18.71	13.5	0.80
red cheddar cheese	17.0	14.8	0.73
water[26]	73.2	8.27	1.00

Table 2. Relaxation parameters obtained from the fitting procedures for the τ–β diagram.

Sample	dimension d_G	Error $\pm e_{dG}$	frequency ω_s (Hz)	Error $\pm e_{\omega s}$	cut off time τ_0 (s)	Error $\pm e_{\tau 0}$
BSA	0.03	2.45	1.92×10^{40}	1.04×10^{44}	3.36×10^{-12}	4.91×10^{-12}
CEWL	0.03	1.60	4.88×10^{39}	1.52×10^{43}	2.67×10^{-12}	2.87×10^{-12}
OVA	0.22	0.89	1.93×10^{14}	6.71×10^{15}	3.66×10^{-12}	1.88×10^{-12}

References

[1] S. Mashimo, N. Miura, and T. Umehara, The Structure of Water and Methanol in p-Dioxane as Determined by Microwave Dielectric Spectroscopy, J. Chem. Phys., 96 (1992) 6358-6361.

[2] U. Kaaze, Complex Permittivity of Water as a Function of Frequency and Temperature, J. Chem. Eng. Data., 34 (1989) 371-374.

[3] R. Buchner, J. Barthel, and J. Stauber, The Dielectric Relaxation of Water between 0°C and 35°C, Chem. Phys. Lett., 306 (1999) 57-63.

[4] T. Fukasawa, T. sato, J. Watanabe, Y. Hama, W. Kunz, and R. Buchner, Relation between Dielectric and Low-Frequency Raman Spectra of Hydrogen-Bond Liquids, Phys. Rev. Lett., 95 (2005) 1-4.

[5] S. Schrodle, G. Hefter, and R. Buchner, Dielectric spectroscopy of hydrogen bond dynamics and microheterogenity of water-dioxane mixtures, J. Phys. Chem., 111 (2007) 5946-5955.

[6] S. Yagihara, N. Shinyashiki, and R. Kita, J. Jpn. Soc. Biorheol., 25 (2011) 2-11.

[7] S. Yagihara and N. Shinyashiki, Dynamics of water Structure in Biological System and Broadband Dielectric Spectroscopy, SEIBUTSU BUUTSURI (Japanese), 44 (2004) 4-9.

[8] S. Yagihara, Fundamental Study and Application of Water Structures in Foods and Related Materials by Broadband Dielectric Spectroscopy (BDS), Nestle Science Promotion Committee Annual Report, (2005) 89-99.

[9] Y. E. Ryabov, Y. Feldman, N. Shinyashiki, and S. Yagihara, The symmetric broadening og the water relaxation peak in polymer-water mixtures and its relaxationship to the hydrophilic and hydrophobic properties of polymers, J. Chem. Phys., 19 (2002) 8610-8615.

[10] Y. E. Ryabov, and Y. Feldman, The Relationship between the scaling parameter and relaxation time for non-exponential relaxation in disordered systems, Fractals., 11 (2003) 173-183.

[11] K. S. Cole, and R. H. Cole, Dispersion and Absorption in Dielectrics, J. Chem. Phys., 9 (1941) 341-351.

[12] R. H. Cole, Evaluation of Dielectric Behavior by Time Domain Spectroscopy. I. Dielectric Response by Real Time Analysis, J. Phys. Chem., 79 (1975) 1459-1469.

[13] R. H. Cole, Evaluation of Dielectric Behavior by Time Domain Spectroscopy. II. Complex Permittivity, J. Phys. Chem., 79 (1975) 1469-1474.

[14] R. H. Cole, S. Mashimo, and P.Winsor IV, Evaluation of Dielectric Behavior by Time Domain Spectroscopy. 3. Precision Difference Methods, J. Phys. Chem., 84 (1980) 786-793.

[15] H. Nakamura, S. Mashimo, and A. Wada, Application of Time Domain Reflectometry Covering a Wide Frequency Range to the Dielectric Study of Polymer Solutions, J. App. Phys., 21 (1982) 467-474.

[16] H. Nakamura, S. Mashimo, and A. Wada, Precise and Easy Method of TDR to Obtain Dielectric Relaxation Spectra in GHz Region, J. App. Phys., 21 (1982) 1022-1024.

[17] J. Z. Bao, C. C. Davis, and M. L. Swicord, Microwave Dielectric Measurements of Erythrocyte Suspensions, Biophys. J., 66 (1994) 2173–2180.

[18] C. Cametti, S. Marchetti, C.M.C. Gambi, and G. Onori, Dielectric relaxation spectroscopy of lysozyme aqueous solutions analysis of the δ-dispersion and the contribution of the hydration water, J. Phys. Chem., 115 (2011)7144-7153.

[19] Farrar, T.C., Becker, E.D., "Pulse and Fourier Transform NMR", Academic Press, New York (1971)

[20] E. O. Stejskal, and J. E. Tanner, Spin Diffusion Measurements: Spin Echoes in the Presence of a Time-Dependent, J. Chem. Phys., 42 (1965) 288-292.

[21] Y. Hayashi, N. Shinyashiki, and S. Yagihara, Dynamical structure of water around biopolymers investigated by microwave dielectric measurements using time domain reflectometry method, J. Non-Cryst. Solids., 305 (2002) 328-332.

[22] S. Yagihara, M. Oyama, A. Inoue, M. Asano, S. sudo, and N. Shinyashiki, Dielectric relaxation measurement and analysis of restricted water structure in rice kernels, Meas. Sci. Technol., 18 (2007) 983-990.

[23] N. Shinyashiki, S. Yagihara, I. Arita, and S. Mashimo, J. Phys. Chem. B, 102 (1998) 3249-3251.

[24] K. Matsumoto, K. Shimazaki, K. Kitamura, R. Kita, N. Shinyashiki, and S. Yagihara, Geometrical Feature of Fractal Structure Expression and Characterization of aqueous Mixtures by Dielectric Spectroscopy, Pros. Sch. Sci. TOKAI UNIV., 43 (2008) 127-143.

[25] K. Shimazaki, K. Matsumoto, R. Kita, N. Shinyashiki, and S. Yagihara, Molecular Dynamics Simulation for Molecular Characterization Analysis of Aqueous Solution of Oligomer, Pros. Sch. Sci. TOKAI UNIV., 45 (2010) 113-129.

[26] U. Kaatze and V. Uhlendorf, The Dielectric Properties of Water at Microwave Frequencies, Zei. Phys. Chem., 126 (1981) 151-165.

Chapter 4

Electric-field penetration depth and dielectric spectroscopy observations of human skin

4.1 Introduction

The characteristics of biological materials are closely related to their water content. Consequently, measurements of the dynamics of water molecules are important in order to understand the structures of hydrous materials and their biological functions. Human skin is composed of three layers termed, sequentially inward from the surface, the epidermis, dermis, and subcutaneous tissue. The water content of the epidermis is lower than that of the dermis,[1, 2] and it behaves as a protective barrier against drying and external irritation. The existence of bound water[3-8] is often suggested, even for human skin.[9] It is not easy to determine the variation of the water content with depth, and measurements are difficult, since water molecules exhibit complex variations on different temporal and spatial scales.

Dielectric measurements using Time Domain Reflectometry (TDR) make it possible to observe relaxation processes that reflect the molecular motions of water. The relaxation process is caused by the formation and disappearance of dynamic clusters of water molecules. For free water molecules, the relaxation time is $\tau = 8.27$ps at 25°C.[10-13] This relaxation time is generally smaller than that of biological macromolecules.

The water content of human skin has been studied extensively by various methods.[14-16] Pratchyapruit *et al*.[17] suggest that the skin of the eyelid remains soft by maintaining sufficient hydration on the skin surface. This example demonstrates that water in the skin is related to biological function.

In our previous studies, we obtained information about the dielectric properties in the stratum corneum of human skin.[18, 19] We also have reported that the healing of human skin after a burn is correlated with the time dependence of its free water content.[20] Applying dielectric measurements of

skin to the area of sports medical science, we were able to observe the large-scale traversal of water molecules into the body during exercise.[21] Dielectric spectroscopy can be employed for non-invasive and non-destructive measurements, including *in vivo* measurements of human skin. These reports clearly indicate that skin measurements using dielectric spectroscopy can provide an important method for characterizing the state of the skin through observations of the molecular behavior of water.

Recently, measurements of the moisture content of skin have been performed using confocal Raman spectroscopy.[22] This experimental technique makes it possible to observe the moisture content at a shallow depth in areas of the skin such as the stratum corneum and epidermis. On the other hand, dielectric spectroscopy yields a value averaged over the penetration depth of the electric field up to the skin surface contacted by the electrode. Furthermore, by increasing the electrode diameter it is possible to obtain information in deeper areas than can be studied with confocal Raman spectroscopy. We have previously reported a comparison of results obtained from these two measuring techniques.[23] Observations of the dynamics of water molecules using dielectric spectroscopy are relevant not only to the water content but also to phenomena such as biological functions and characteristics *in vivo*. Therefore, dielectric spectroscopy is appropriate for *in vivo* measurements.

In dielectric spectroscopy of the skin, it is important to know which and how dielectric information in depth is obtained for substances with different water contents. Accordingly, we have examined the characteristic electric-field penetration depths of a two-layer dielectric model using water and a Teflon block.[18, 24, 25] The penetration depth obtained from such measurements depends on the outer diameter of the coaxial electrode. However, the electrode diameter was only one of the unknowns in previous research. In this study, we have used TDR with open-ended coaxial electrodes having different electric-field penetration depths to perform dielectric measurements of an acetone-Teflon double layer and of human skin from various parts of the body, in order to study the distribution of water content in the human skin.

4.2 Materials and Methods

4.2.1 Acetone-Teflon double-layer system for the characterization of coaxial electrodes

A block diagram of the apparatus employed for the characterization of coaxial electrodes is shown in Figure 1. We purchased a flat, 10 mm-thick Teflon sheet with static permittivity ε_r=2.1 from FLON INDUSTRY. We placed a glass bottle on a jack and filled the bottle with acetone (with static

permittivity ε_a=21 at 20°C[26]). We then placed a Teflon sample in the bottom of the bottle to form an acetone-Teflon double-layer system. We first placed the end of the electrode into contact with the surface of the Teflon, and we then changed the vertical distance between the Teflon surface and the end of the electrode gradually using the jack while we performed the dielectric measurements. We determined the distance using a digital indicator. We used 50Ω, semi-rigid coaxial cables (SUHNER) with outer diameters of 0.86, 1.19, 2.20, 3.56, and 6.35 mm as the electrodes for the TDR measurements at room temperature (20.0±0.5°C).

4.2.2 Human-skin measurements on various parts of a body

We measured various parts of the bodies of two examinees (A: male, age 24; B: female, age 26) using TDR, with the same electrodes as we used for the acetone-Teflon double-layer measurements at room temperature, 20.0±0.5°C, with humidity 50±1%. The body parts we measured were the cheek, the palm side of the forearm, the palm, and the sole of the foot. We also used TDR to measure the same body parts of two other examinees (C: male, age 24; D: female, age 22) with an electrode having an outer diameter of 2.2 mm. We washed the measured body parts with soap and wiped them with Kimwipe before the measurements. In order to restore the state of the skin prior to the measurements, we asked each examinee to remain still in the examining room for 30 minutes so as not to sweat.

4.2.3 Time-Domain Reflectometry Measurements

We employed a digitizing oscilloscope mainframe (HP 54120B) with a four-channel test set (HP 54124A) as the TDR system.[27-31] This enabled us to make dielectric measurements—especially for the relaxation process due to the molecular dynamics of free water—over the frequency range from 100MHz to 30GHz. We observed the reflected microwave signals, which include information about the dielectric properties of the sample in response to the incident step pulse.

The complex permittivity of the sample can be expressed by the basic equation of the TDR method:[27-29]

$$\varepsilon* = \frac{c'}{j\omega\gamma d} \frac{v_0 - r}{v_0 + r} X \cot X \tag{4.1}$$

where c' is the speed of propagation in the coaxial line, v_0 and r are the Laplace transforms of the incident and reflected pulse waveforms, $X \cot X$ takes into account propagation and multiple reflections in the sample and the coaxial-line geometry, and γd is a correction coefficient. There is reference method[27-29] using the difference between the reflected wave of a standard sample having a known complex dielectric constant and the reflected wave of an unknown sample, which was used because it is more accurate.[27-29] The values of the correction coefficients γd are listed for each

electrode in Table 1. We also calibrated the open-ended probes using standard samples (air, acetone, and water) with known dielectric properties.

We performed the TDR measurements using a contact-type coaxial electrode with an open-ended tip in direct contact with the object to be measured. The TDR measurement requires an electric field generated around the tip of the electrode. The electric lines of force reach from the central to the outer conductors through the interior of the object. The dielectric information is obtained in the region where a relatively large electric field is applied around the electrode tip. Therefore, the electric lines of force necessarily depend on the diameter of the electrode. In this report, we use measurements of the dielectric information averaged over the penetration depth of the electric field as the basis for discussing the layered structure of the human skin.

4.3 Results

4.3.1 Acetone-Teflon double-layer system

Figure 2 shows the relationship between the static dielectric constant ε_s and the distance l between the electrode and the Teflon surface for electrodes with outer diameters of 0.86, 1.19, 2.20, 3.56, and 6.35 mm. The ε_s values increase with increasing l, and they asymptotically approach the value for acetone. The dielectric constant thus obtained is larger than ε_t=2.1, even when the end of electrode just touches the Teflon surface (l=0), because there remains a small gap filled with acetone. The variation of the dielectric constant with position thus obtained shows exponential-like decays.

4.3.2 Human-skin measurements

We used electrodes with various outer diameters to measure various parts of the body, and we observed the respective dielectric relaxation curves. We found the dielectric constant to be small when the electrode diameter was small. In addition, we obtained smaller values of the dielectric constant for body parts with larger skin thicknesses.

4.4 Discussion

4.4.1 Characterization of the penetration depth of the electric field

The distance dependence shown in Figure 2 can be expressed approximately by the following equation:[24, 25]

$$\varepsilon_s = \varepsilon_t - \left\{\varepsilon_a - \varepsilon_t \left[1 - exp\left(-\frac{l}{l_0}\right)\right]\right\} , \qquad (4.2)$$

where ε_a is the dielectric constant of acetone, and l_0 is defined as the penetration depth of the electric field. The penetration depth has a characteristic value for each electrode, which is determined from Eq. (4.2). The penetration depth is an average value, and some parts of the electric field lines reach deeper regions.

The dielectric constant ε_s and the distance l thus obtained are listed in Tables 2-6. As noted in section 3.1 above, when the end of the electrode just touches the Teflon surface (l=0), the dielectric constant obtained from the measurements is larger than ε_t=2.1 because of acetone in the gap between the end of the electrode and the Teflon surface. In our previous research, we pointed out that this does not affect our determination of the penetration depth, as explained below.[24, 25] Eq. (4.2) can be rewritten as

$$\varepsilon_a - \varepsilon_s = (\varepsilon_a - \varepsilon_t)exp\left(-\frac{l}{l_0}\right) , \qquad (4.3)$$

which corresponds to a straight line in the semi-logarithmic plot shown in Figure 3. We obtained these straight lines from least-squares fits to the exponential function given by Eq. (4.3) for each electrode diameter. The slope of this straight line gives the electric-field penetration depth l_0. The penetration depth so obtained for each electrode diameter is listed in Table 7. The penetration depth clearly increases with increasing electrode diameter. This diameter-dependence is reasonable, because the electric-field lines from the central to the outer conductors are longer for electrodes with larger outer diameters.

4.4.2 Human skin observed using dielectric spectroscopy

Dielectric relaxation spectra obtained from TDR measurements of the palm side of the forearm using electrodes of various diameters are shown in Figure 4. The curves show at least two relaxation processes, one in the frequency region above 10GHz and the other below 1GHz. Figure 4 also shows that larger dielectric constants and losses are obtained for electrodes with larger diameters.

The dielectric relaxation curves thus obtained can be described by the sum of two Cole-Cole equations:

$$\varepsilon^* = \varepsilon_\infty + \frac{\Delta\varepsilon_h}{1+(j\omega\tau_h)^{\beta_h}} + \frac{\Delta\varepsilon_l}{1+(j\omega\tau_l)^{\beta_l}} , \qquad (4.4)$$

where ε^* is the complex dielectric permittivity, ε_∞ is the high-frequency limit of the dielectric

constant, $\Delta\varepsilon$ is the relaxation strength, τ is the relaxation time, β is the relaxation-time distribution parameter, and h and l indicate the higher and lower relaxation processes, respectively. A typical result of a fit of Eq. (4.4) to the relaxation processes obtained for the palm side of the forearm using the 2.20 mm-diameter electrode is shown in Figure 5. It is reasonable to assume that the h process results from the reorientation of free water molecules and that the l process results from a superposition of multiple factors, such as interfacial polarization, bound water, and local chain motions of macromolecules, as indicated in our previous work.[20]

Figures 6 and 7 show the relationship between the relaxation strength of the h process and the thickness d of the epidermis for two examinees.   We obtained the thickness of the epidermis at the various measurement sites from the literature on anatomically based thicknesses,[32] as listed in Table 8. The actual thickness of the epidermis for each examinee will in fact be different. Plots of the logarithm of $\Delta\varepsilon$ obtained for each electrode, however, showed straight lines against d, as shown in Figures 6 and 7. Though the relaxation strength depends on both the examinee and the physical conditions, Figures 6 and 7 indicate that this linear dependence is common and suggests that any such influence is small compared with the difference among the measured body parts.

In addition, we found that the thickness of the epidermis was neither extremely thin nor extremely thick compared to the average value for each measured body part, even for examinees. The straight lines show the dependence on the thickness of the body part of each examinee. Figure 7 shows that the straight lines for electrodes with larger penetration depths generally have shallower slopes and larger values of the relaxation strength $\Delta\varepsilon$ than those shown in Figure 6. This means that the contribution of dermis with high water content is smaller in Figure 6. Therefore, it is conceivable that examinee A (Figure 6) has a thicker epidermis than examinee B (Figure 7).

The vertical axes of Figures 8 and 9 represent the moisture content of the skin for each body part obtained by all electrodes, with different electric-field penetration depths l_0. Electrodes with larger l_0 values apparently probe regions with larger moisture content, since the ratio of water-rich dermis to water-poor epidermis increases with l_0. These curves show that examinee A exhibited less change in water content, compared with examinee B, because of the former's thicker epidermis. For examinee A, with a thicker epidermis, even if the penetration depth of the electrode increases, the apparent moisture content does not increase much. In other words, the present technique of dielectric spectroscopy can determine the unknown thickness of the epidermis of any body part.

Figure 10 shows the relationship between the relaxation strength of the h process and the thickness of the epidermis for the 2.20 mm-diameter electrode for four examinees. We found that for a given electrode diameter the difference in the slope depends on the examinee. This difference in the slope of the straight line expresses the difference in the thickness of the epidermis for each examinee. These results also depend on the physical condition of the day, however, although the effect is small compared to the difference between different body parts. Even if the thickness of the epidermis

depends on the examinee, it is neither extremely thin nor extremely thick compared to the average value for each body part, as in Figures 6 and 7. Thus, the relative thickness of each body part exhibits a linear dependency for each examinee. The thickness of human skin thus does not change drastically between different parts of the body. These results demonstrate that our present approach can be an effective tool for a detailed assessment of human skin.

4.5 Conclusion

We determined the penetration depths of the electric fields of open-ended coaxial electrodes of various diameters that we used for dielectric measurements. The penetration depth increases with increasing electrode diameter. We found from systematic measurements with various electrodes that the epidermis has a more limited water content than the dermis. The logarithm of the relaxation strength obtained for each electrode follows a linear relationship with the thickness of the epidermis in the different examinees. The differences in slope of the straight lines correspond to differences in the thickness of the epidermis of the examinees. Even if the thickness of the epidermis depends on the examinee, the relative thickness of each part generally offers the linear dependency, as it is neither extremely thin nor extremely thick compared to the average value of each part. These characteristic behaviors suggest a methodology for a detailed assessment of the skin using the present analysis of systematic dielectric measurements with coaxial electrodes having different penetration depths.

Table 1. Values of correction coefficients.

ϕ [mm]	0.86	1.19	2.20	3.56	6.35
γd [mm]	0.059	0.082	0.15	0.29	0.46

Table 2. Parameters for an electrode with an outer diameter of 0.86 mm.

l [mm]	ε_s	$\ln(\varepsilon_a - \varepsilon_s)$
0.00	5.43	2.75
0.01	11.04	2.30
0.02	13.91	1.96
0.03	16.13	1.58
0.04	15.91	1.63
0.05	16.53	1.50
0.06	16.40	1.53
0.08	18.83	0.78
0.10	18.56	0.89
0.20	20.70	-1.21
0.30	20.97	-3.44

Table 3. Parameters for an electrode with an outer diameter of 1.19 mm.

l [mm]	ε_s	$\ln(\varepsilon_a - \varepsilon_s)$
0.00	5.11	2.77
0.01	6.82	2.65
0.02	7.81	2.58
0.03	8.58	2.52
0.04	8.81	2.50
0.05	9.66	2.43
0.10	13.34	2.04
0.15	15.33	1.74
0.20	18.91	0.74
0.25	19.07	0.66

Table 4. Parameters for an electrode with an outer diameter of 2.20 mm.

l [mm]	ε_s	$\ln(\varepsilon_a - \varepsilon_s)$
0.00	6.62	2.67
0.02	9.89	2.41
0.04	13.41	2.03
0.06	15.36	1.73
0.08	16.88	1.42
0.10	17.00	1.39
0.15	17.63	1.21
0.20	18.53	0.90
0.25	18.93	0.73
0.30	19.57	0.36
0.35	19.83	0.16
0.40	20.12	-0.13
0.45	20.22	-0.25
0.50	20.60	-0.92
0.60	21.10	-
0.70	20.95	-3.00
0.80	21.19	-
0.90	21.07	-

Table 5. Parameters for an electrode with an outer diameter of 3.58 mm.

l [mm]	ε_s	$\ln(\varepsilon_a-\varepsilon_s)$
0.00	5.27	2.76
0.02	10.11	2.39
0.04	10.89	2.31
0.06	11.22	2.28
0.08	11.49	2.25
0.10	11.88	2.21
0.15	13.50	2.01
0.20	14.74	1.83
0.25	15.12	1.77
0.30	15.90	1.63
0.35	16.89	1.41
0.40	17.55	1.24
0.45	17.98	1.11
0.50	18.1	1.06
0.60	19.15	0.62
0.70	19.51	0.40
0.80	19.7	0.26
0.90	20.24	-0.27
1.00	20.74	-1.35

Table 6. Parameters for an electrode with an outer diameter of 6.35 mm.

l [mm]	ε_s	$\ln(\varepsilon_a-\varepsilon_s)$
0.00	3.90	2.84
0.01	4.35	2.81
0.02	4.85	2.78
0.03	5.08	2.77
0.04	5.51	2.74
0.05	5.97	2.71
0.10	7.15	2.63
0.15	8.45	2.53
0.20	9.48	2.44
0.25	10.16	2.38
0.30	10.76	2.33
0.40	12.74	2.11
0.50	13.98	1.95
0.60	15.43	1.72
0.70	16.49	1.51
0.80	17.47	1.26
0.90	18.14	1.05
1.00	18.90	0.74
1.20	19.69	0.27

Table 7. Penetration depth of the electric field

ϕ [mm]	0.86	1.19	2.20	3.56	6.35
l_0 [mm]	0.052	0.11	0.15	0.30	0.49

Table 8. Thickness of the epidermis of different body parts, from Ref. 32.

Body parts	Thickness of epidermis [mm]
cheek	0.042
palm side of the forearm	0.086
palm	0.145
sole of the foot	0.185
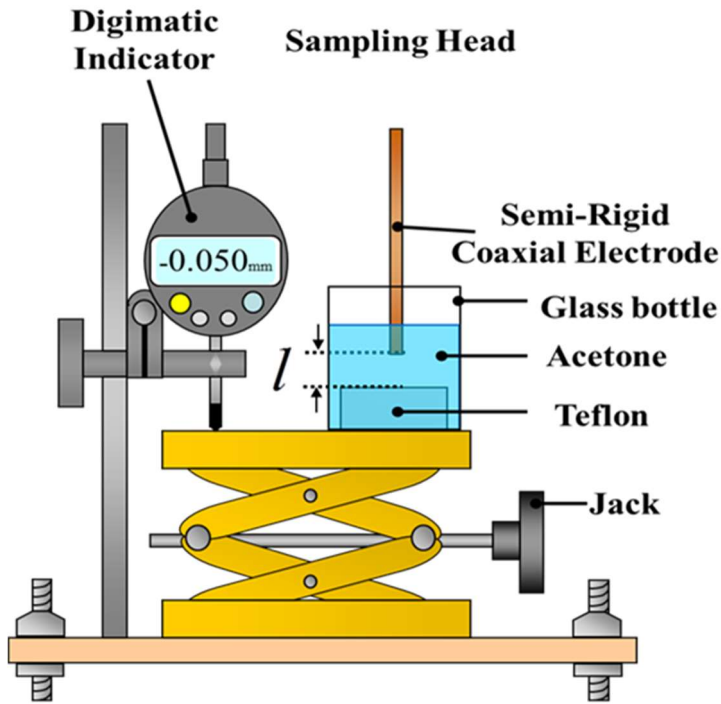
Figure 1. Block diagram used for the acetone-Teflon double-layer measurements.
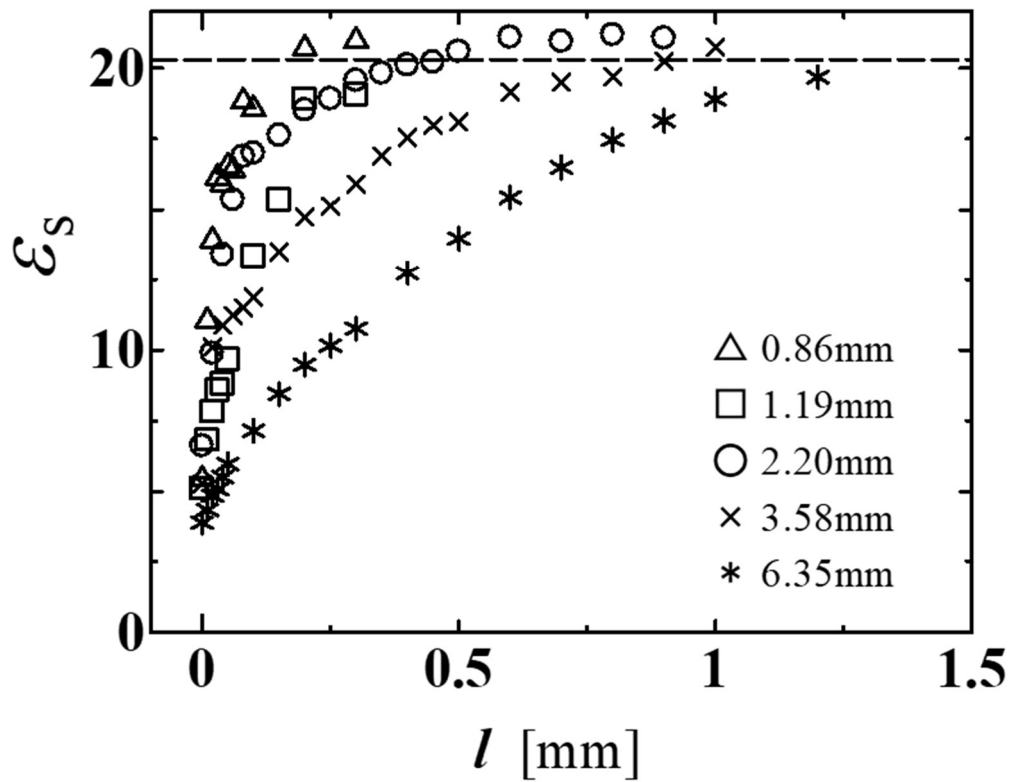
Figure 2. Relationship of the measured dielectric constant to the distance between the Teflon surface and the electrode, for outer electrode diameters of 0.86, 1.19, 2.20, 3.58, and 6.35 mm.
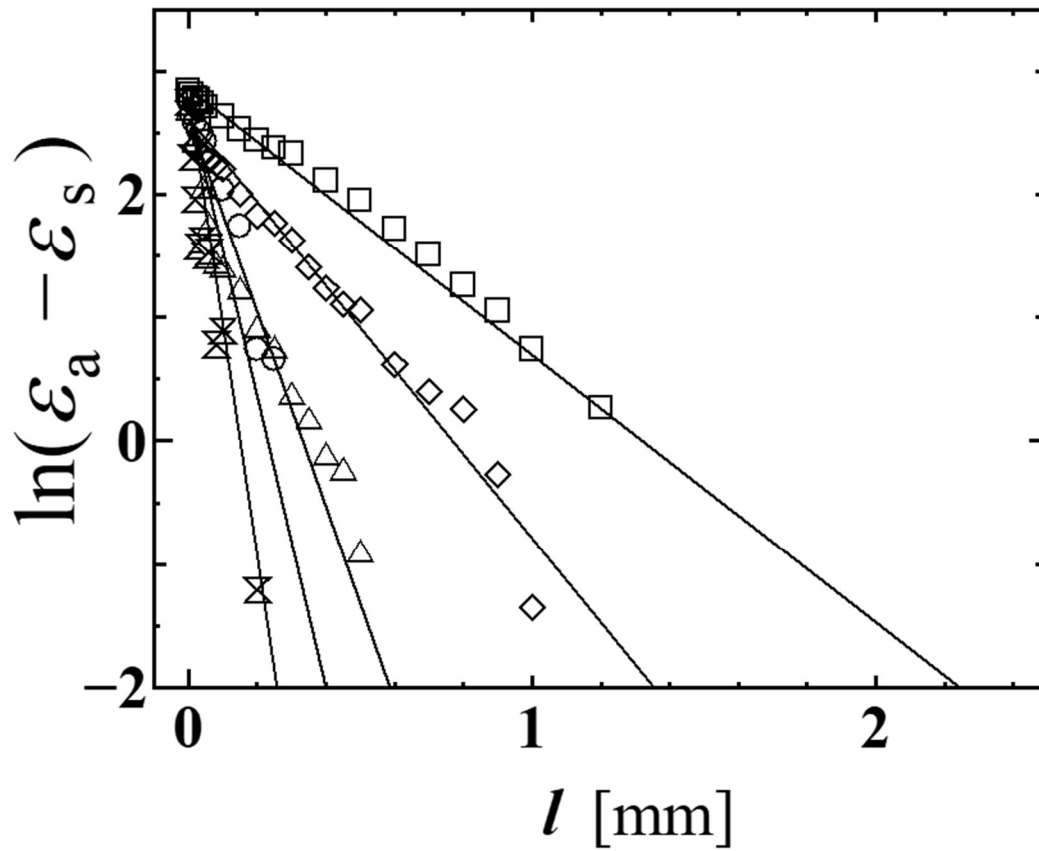
Figure 3. Approximation lines in semi-logarithmic plots for various electrodes. The symbols are the same as in Fig. 2.
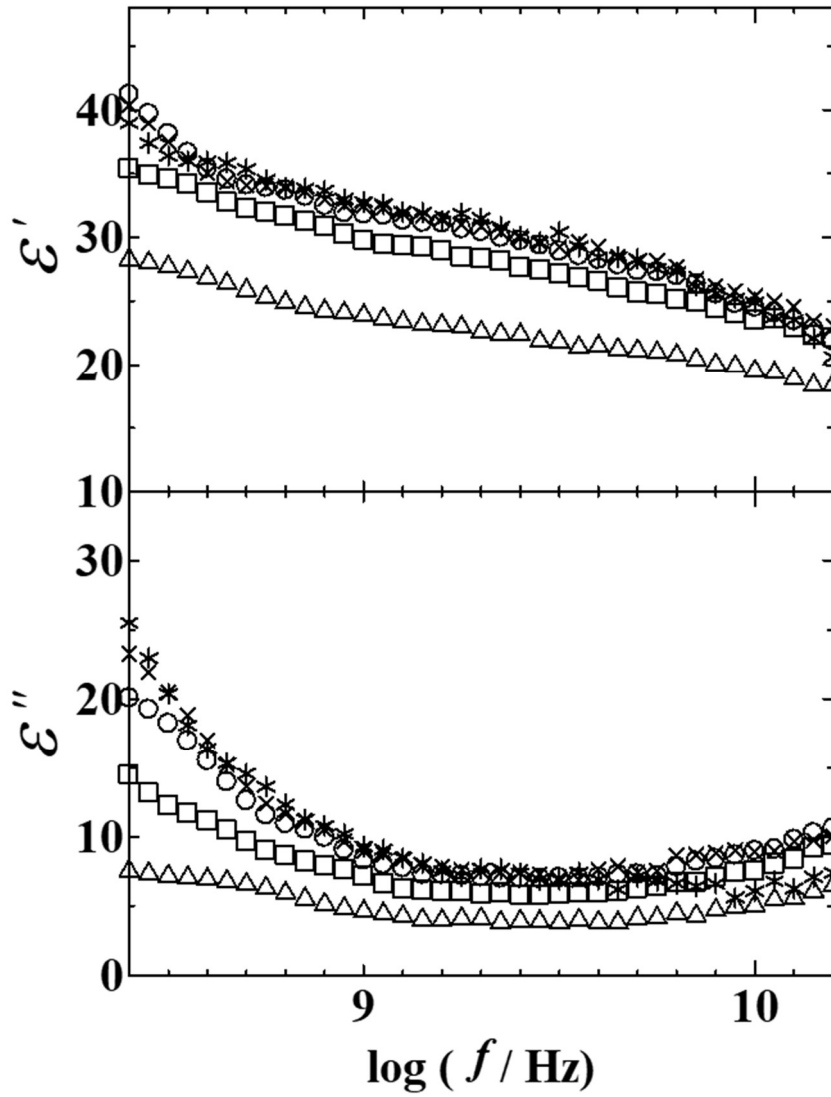
Figure 4. Frequency dependence of the complex dielectric constant of human skin, obtained using various probe diameters. The symbols are the same as in Fig. 2.
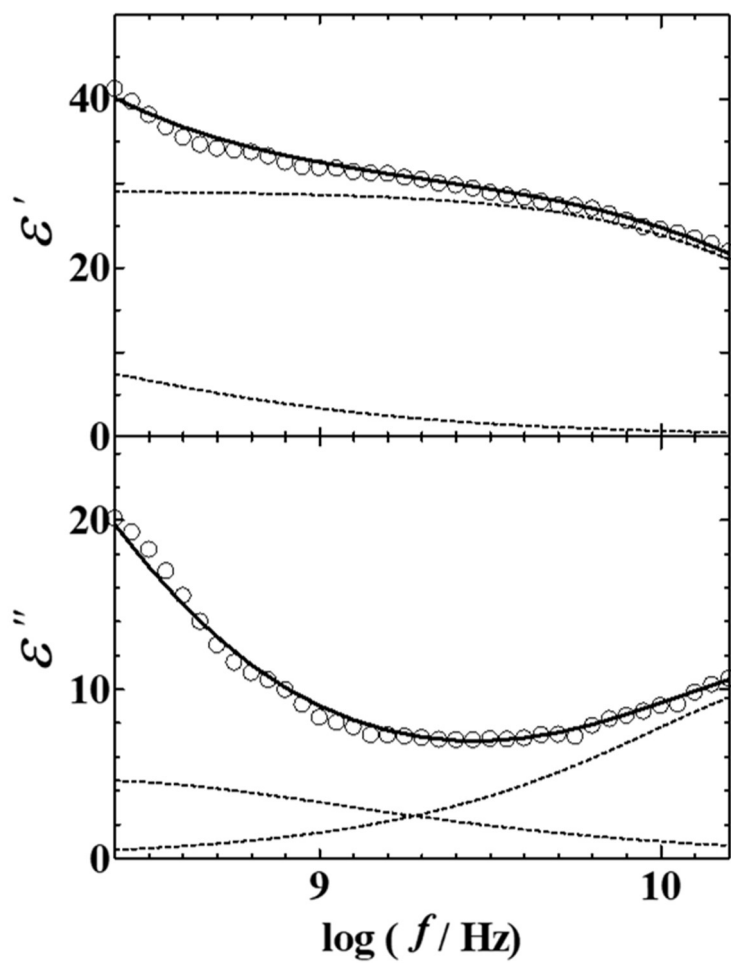
Figure 5. Frequency dependence of the complex dielectric constant obtained with an electrode having an outer diameter of 2.20 mm. The solid lines correspond to the two relaxation processes obtained from the fitting procedure.
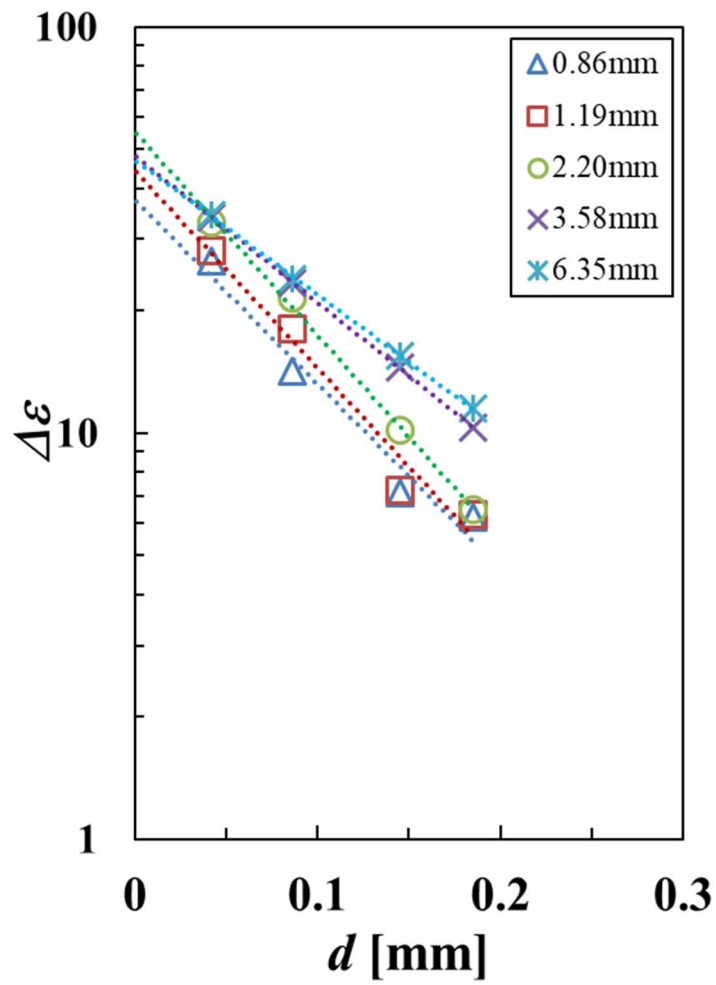
Figure 6. Relationship of the relaxation strength and the thickness of the epidermis for probes with outer diameters of 0.86, 1.19, 2.20, 3.58, and 6.35 mm [examinee A: male].
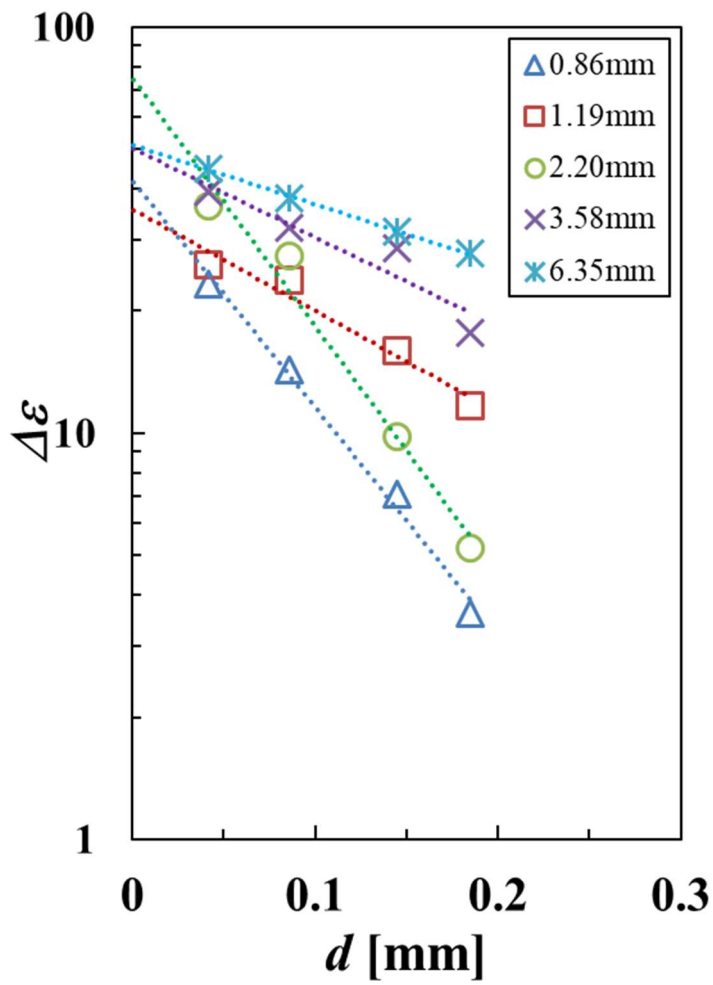
Figure 7. Relationship of the relaxation strength and the thickness of the epidermis for probes with outer diameters of 0.86, 1.19, 2.20, 3.58, and 6.35 mm [examinee B: female].
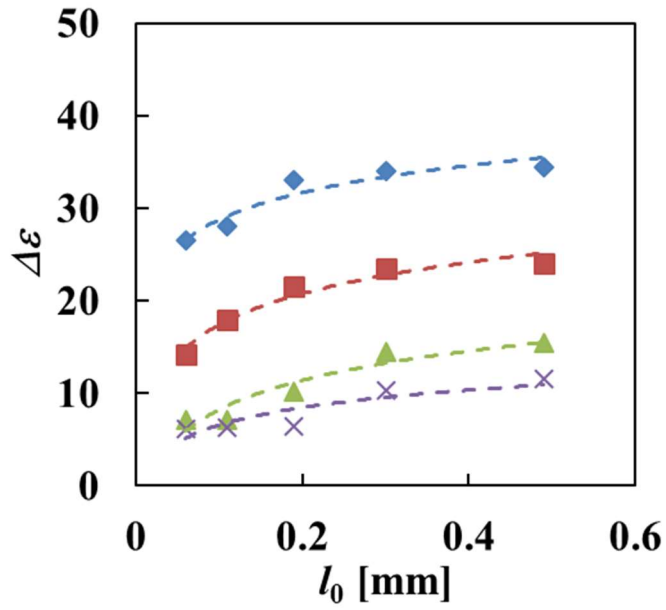
Figure 8. The moisture content of the skin of the cheek (◊), palm side of the forearm (□), palm (△), and the sole of the foot (×) obtained from electrodes with different values of l_0 [examinee A: male].
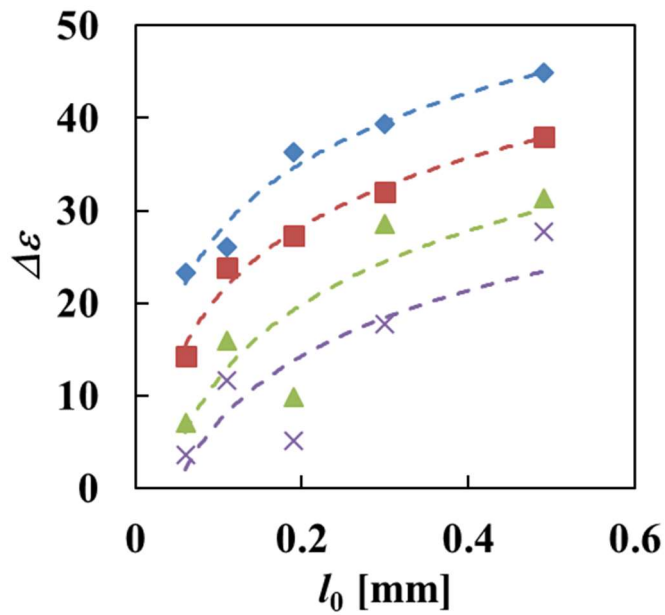

Figure 9. The moisture content of the skin of the cheek (◊), palm side of the forearm (□), palm (△), and the sole of the foot (×) obtained from electrodes with different values of l_0 [examinee B: female].
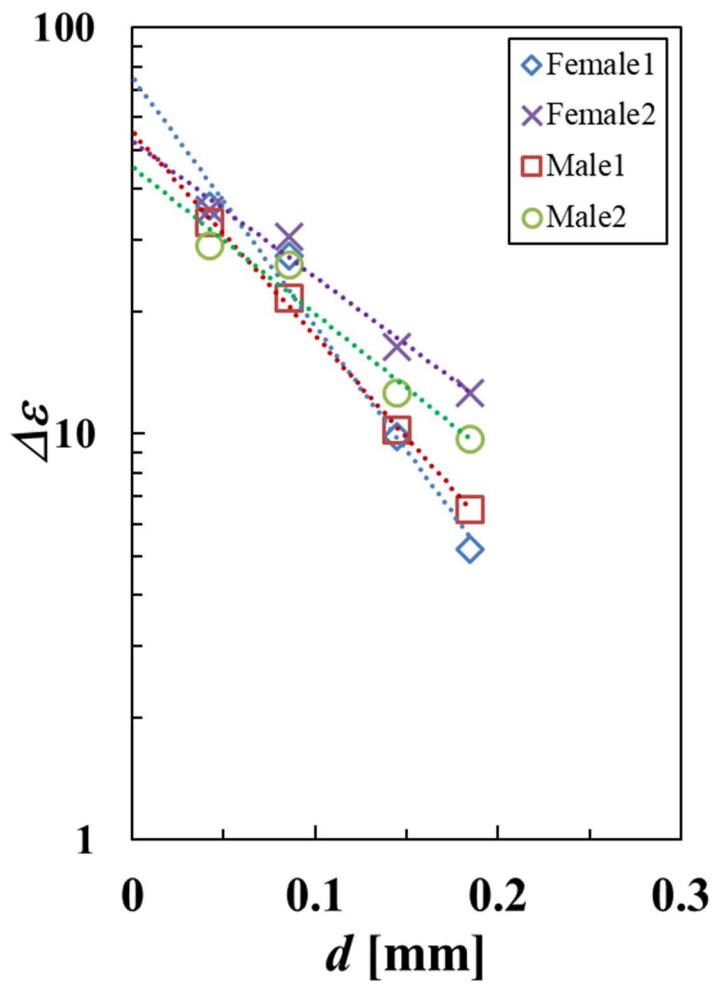
Figure 10. Relationship of the relaxation strength to the thickness of the epidermis for the probe with 2.2 mm outer diameter for four examinees, two males and two females.

References

[1] T. Abe, Water and the skin, J. Jpn. Oil. Chem. Soc., 34 (1985) 413-419.

[2] H. Tagami, Electrical measurement of the hydration state of the skin surface *in vivo*, Br. J. Dermatol., 171 (2014) 29-33.

[3] Umehara T, Kuwabara S, Mashimo S, et al. Dielectric study on hydration of B-, A-, and Z-DNA. Biopolymers 30 (1990) 649-656.

[4] Shinyashiki N, Asaka N, Mashimo S, et al. Microwave dielectric study on hydration of moist collagen, Biopolymers, 20 (1990) 1185-1191.

[5] Miura N, Asaka N, Shinyashiki N, et al. Microwave dielectric study on bound water of globule proteins in aqueous solution, Biopolymers, 34 (1994) 357-364.

[6] Miura N, Hayashi Y, Shinyashiki N, et al. Observation of unfreezable water in aqueous solution of globule protein by microwave dielectric measurement, Biopolymers, 36 (1995) 9-16.

[7] Miura N, Hayashi Y, Mashimo S. Hinge-bending deformation of enzyme observed by microwave dielectric measurement, Biopolymers, 39 (1996) 183-187.

[8] Hayashi Y, Miura N, Isobe J, et al. Molecular dynamics of hinge-bending motion of IgG vanishing with hydrolysis by papain, Biophys. J., 79 (2000) 1023-1029.

[9] Boireau-Adamezyk E, Baillet-Guffroy A, Stamatas GN. Mobility of water molecules in the stratum corneum: effects of age and chronic exposure to the environment, J. Invest. Dermatol., 134 (2014) 2046-2049.

[10] Kaaze U. Complex permittivity of water as a function of frequency and temperature, J. Chem. Eng. Data., 34 (1989) 371-374.

[11] Buchner R, Barthel J, Stauber J. The dielectric relaxation of water between 0°C and 35°C, Chem. Phys. Lett., 306 (1999) 57-63.

[12] Fukasawa T, Sato T, Watanabe J, et al. Relation between dielectric and low-frequency Raman spectra of hydrogen-bond liquids, Phys. Rev. Lett., 95 (2005) 1-4.

[13] Schrodle S, Hefter G, Buchner R. Dielectric spectroscopy of hydrogen bond dynamics and microheterogenity of water-dioxane mixtures, J. Phys. Chem., 111 (2007) 5946-5955.

[14] Tagami H, Ohi M, Iwatsuki K, et al. Evaluation of skin surface hydration *in vivo* by electrical measurement, J. Invest. Dermatol., 75 (1980) 500-507.

[15] Naito S. A new method of measuring stratum corneum water content by dielectric analysis in microwave region, J. Jpn. Cosmet. Sci. Soc., 22 (1998) 1-7.

[16] Mayrovitz HN, Bernal M, Brlit F, et al. Biophysical measures of skin tissue water: variations within and among anatomical sites and correlations between measures, Skin. Res. Technol., 19 (2013) 47-54.

[17] Pratchyapruit W, Kikuchi K, Gritiyarangasan P, et al. Functional analyses of the eyelid skin constituting the most soft and smooth area on the face: contribution of its remarkably large

superficial corneocytes to effective water-holding capacity of the stratum corneum, Skin. Res. Technol., 13 (2007) 169-175.

[18] Naito S, Hoshi M, Mashimo S. A method of measuring surface permittivity by microwave dielectric analysis, Rev. Sci. Instrum. 67 (1996) 3633-3641.

[19] Naito S. Hoshi M. Yagihara S. Microwave dielectric analysis of human stratum corneum in vivo, Biochim. Biophys. Acta., 1381 (1998) 293-304.

[20] Hayashi Y, Miura N, Shinyashiki N, et al. Free water content and monitoring of healing processes of skin burns studied by microwave dielectric spectroscopy *in vivo*, Phys. Med. Biol., 50 (2005) 599-612.

[21] Hashimoto T, Yamamura M, Yagihara S, et al. Build up of the epidermis after excise, Tokai. J. Sports. Med. Sci., 15 (2003) 67-72.

[22] Hirao T, Egawa M, Yamashita T. Recent advances in technologies for measurement of the skin, J. Surf. Sci. Soc. Jpn. 35 (2014) 17-22.

[23] Sato S, Maruyama Y, Kamata H, et al. Evaluation of water measurement techniques for human skin by dielectric spectroscopy and confocal Raman spectroscopy, Trans. Mat. Res. Soc. Japan., 40 (2015) 133-136.

[24] Hashimoto M, Goto T, Shinyashiki N, et al. Interpretation of hydration structure of human skin from analysis of electrodes used in dielectric spectroscopy, Tokai. J. Sports. Med. Sci., 19 (2007) 52-62.

[25] Goto T, Hashimoto M, Shinyashiki N, et al. Dielectric study on distribution of water in human skin, Trans. Mat. Res. Soc. Japan., 31 (2006) 771-774.

[26] Barthel J, Buchner R. High frequency permittivity and its use in the investigation of solution properties, Pure. Appl. Chem., 63 (1991) 1473-1482.

[27] Cole RH. Evaluation of dielectric behavior by time-domain spectroscopy. I. Dielectric response by real time analysis, J. Phys. Chem., 79 (1975) 1459-1469.

[28] Cole RH. Evaluation of dielectric behavior by time-domain spectroscopy. II. complex permittivity, J. Phys. Chem., 79 (1975) 1469-1474.

[29] Cole RH, Mashimo S, Winsor P. IV, Evaluation of dielectric behavior by time-domain spectroscopy. 3. precision difference methods, J. Phys. Chem., 84 (1980) 786-793.

[30] Nakamura H, Mashimo S, Wada A. Application of time-domain reflectometry covering a wide frequency range to the dielectric study of polymer solutions, J. App. Phys., 21 (1982) 467-474.

[31] Nakamura H, Mashimo S, Wada A. Precise and easy method of TDR to obtain dielectric relaxation spectra in GHz region, J. App. Phys., 21 (1982) 1022-1024.

[32] Yazawa S. Comparative study of skin tissue in various parts of human body [Translated from Japanese.], Med. Research., 7 (1933) 1805-1846.

Chapter 5

Comparison of Biometric Dielectric Spectroscopy and Blood Flow Measurements

5.1 Introduction

Inside the living tissue, water structures taking complex high-order structures through hydrogen bonds with various biological molecules are constantly ever-changing in the picosecond time domain. These have been observed in the GHz frequency range, and we have been conducting research focusing on *in vivo* water by noninvasive measurements using dielectric spectroscopy. We have analyzed function expression mechanisms *in vivo* by non-invasive measurements with observation of the healing process of skin after burns [1], observation of changes in free water amount in the epidermis during exercise applied to sports medicine science [2], electric field analysis using dielectric models and various parts of the body for skin measurements [3-5], and so on. It has been also found that the electric field analysis of the open-end coaxial electrode can provide depth information from the skin surface.

Blood consists of cell components of red blood cells (RBCs) and white blood cells, platelets, and plasma. It is reported that RBCs having particles of micrometer order size cause Maxwell-Wagner interface polarization, which can be observed by dielectric measurements in the 1 MHz frequency region [6]. Blood flow measurements *in vivo* using open-ended electrodes have also shown that one of the observed relaxation processes is attributed to blood flow information [7].

A blood test can diagnose illness as a relatively light physical examination, though the test involves pain during blood collection. However, blood tests have a relatively low physical burden, even if it is relatively low as compared to other detailed examinations likes endoscopes. If the condition of blood can be observed by noninvasive and nondestructive dielectric measurement, the burden can be further reduced. More detailed discussion of the relaxation process observed in dielectric measurement is necessary for the application.

In this study, in order to evaluate blood flow by dielectric spectroscopy measurements, blood flow measurements *in vivo* were performed using ultrasonic blood flow meter and laser blood flow meter in addition to dielectric measurements. It was discussed whether dielectric spectroscopy is also useful for blood flow measurements in living body compared with other methods.

5.2 Experimental

5.2.1 Examinees

Four examinees' normal data are shown in the Table 1. Each measurement was started after sprint stress in the room (temperature: 20.0±0.5°C, humidity: 50.0±0.5%).

5.2.2 Dielectric Measurements

The dielectric measurements were performed in the frequency range from 40 Hz to 110 MHz using a precision impedance analyzer (4294A, Agilent Technologies) and open-ended coaxial electrodes with the outer diameter 6.3 mm for skin above the wrist artery.

5.2.3 Laser Blood Flow Meter [8]

The microcirculatory blood flow about 1 mm below the skin surface was measured using a laser blood flow meter (OMEGAWAVE, INC.) with 780 nm semiconductor laser. The measurement part was the fingertip of the left hand. Parameters obtained from the laser blood flow meter are values corresponding to the tissue blood volume, blood volume, and blood flow velocity. The laser blood flow meter processes the scattered light from the RBCs and detects the RBC number density and its velocity. The tissue blood flow rate is expressed as a value corresponding to the amount of blood flowing into a living tissue weight of 100 g per unit time. RBC number density corresponds to the blood volume, and the RBC flow velocity corresponds to the blood flow velocity.

5.2.4 Ultrasonic Blood Flow Meter

Mean blood flow velocity was measured using the commercially available ultrasonic blood flow meter (ES-100V3, Hadeco) with 8MHz probe for skin above the wrist artery. This device measures the velocity of blood flow from the Doppler Effect.

5.3 Results and discussion

The dielectric relaxation curves obtained before and after sprint for two examinees are shown, respectively, in Figure 1, where the real part ε' and the imaginary part ε'' of the complex permittivity are plotted as a function of frequency f. It was confirmed that both examinees A and B returned to

the dielectric relaxation curve before sprint with the change over time. It was found from the previous research that the spectrum shown in the 1MHz region reflects the interfacial polarization of the erythrocyte membrane [7].

Dielectric relaxation curved thus obtained could be described by the summation of four Cole-Cole equations [9] as

$$\varepsilon^* = \varepsilon' - j\varepsilon''$$

$$= \varepsilon_\infty + \sum_k^{I,II,III,IV} \frac{\Delta\varepsilon_k}{1+(j\omega\tau_k)^\beta} - j\frac{\sigma_{DC}}{\varepsilon_0\omega}, \qquad (5.1)$$

where ε^* is the complex dielectric permittivity, ε_∞ is the high frequency limit of the dielectric constant, $\Delta\varepsilon$ is the relaxation strength, τ is the relaxation time, β is the relaxation time distribution parameter, σ is the direct current (dc) conductivity, and ε_0 is the dielectric constant of vacuum, and I, II, III, and IV indicate respective processes in order from the higher frequency side. These processes are shown in Figure 2.

Figure 3 shows the time dependences of relaxation parameters of relaxation process I after the sprint obtained from fitting procedures of Eq. (5.1) to the relaxation curve for each examinee. The dashed line shows the values of each examinee's relaxation parameters before the sprint. The relaxation strength $\Delta\varepsilon$ and the relaxation time τ are immediately increased after the sprint and returned to the resting value obtained before the sprint with the elapsed time for each examinee. Since relaxation process I shows the interfacial polarization of RBCs and fine blood vessels [7], an increase in the relaxation strength due to the sprint primarily indicates an increase in the RBC number. In addition, the relaxation time corresponds to the time scale of the polarization formation. So, the relaxation time of the interface polarization are corresponding to the length scale of the interface [10]. Therefore, it is considered that the interfacial polarization increased with the RBCs number due to the sprint are then decreased to a constant value with the elapsed time after the sprint, although the relaxation time distribution parameter β showed respective values for examinees.

Comparing the relaxation strengths obtained for two examinees, the female examinee B has a smaller value than that for the male examinee A. In general, the average number of RBCs is about 10% less for female than that for male [11]. The lower relaxation intensity for examinee B compared to examinee A is considered to reflect the difference in the number of RBCs due to the gender difference. The RBC count can be obtained also from the dielectric measurements.

Figure 4 shows the time dependence of the blood flow parameter ratio by laser blood flow meter for examinee B. The vertical axis represents the ratio to the value at rest and indicates the initial values were higher than 100% after the sprint. Since the blood volume corresponds to the RBC count density, it was confirmed that blood vessels dilated, and the blood volume was increased by the sprint.

Figure 5 shows the time dependence of the mean blood flow velocity and the pulse after the sprint

for three examinees obtained by the ultrasonic blood flow meter. It was confirmed that the pulse of each examinee gradually returned to the values obtained before sprinting. The relationship between the pulse and the mean blood flow velocity is shown in Figure 6. It was found that the area plotted for each examinee was different. This result indicates that changes in the mean blood flow velocity due to the sprint reflect individual situations.

Figures 7a and 7b show the comparison of the relaxation strength obtained from dielectric measurements from to mean blood flow velocity and pulse rate obtained with an ultrasonic blood flow meter, respectively, for examinee B. Both the relaxation strength and pulse increased by the sprint and returned to resting values. The higher pulse delivered more blood, as confirmed by the increase in the relaxation strength corresponding to an increase in the number of RBCs. In addition, the mean blood flow velocity becomes slower after the sprint and returns to the resting velocity with the elapsed time, because the blood vessels are considered to be dilated by the sprint compared to the rest. It was found that the results of dielectric measurement and ultrasonic blood flow meter had well correlated each other.

Comparisons of the relaxation process I due to the interface polarization of the RBCs and fine blood vessels with results obtained from the ultrasonic blood flow meter and laser blood flow meter suggest a large possibility of the blood state evaluation in a living body by dielectric spectroscopy. In addition to the relaxation process I, other relaxation processes observed in dielectric measurements contain more information. By revealing these details, more blood information can be obtained than other approaches. It can be expected that dielectric spectroscopy will be able to obtain more detailed blood information from *in vivo* measurements in near future.

5.4 Conclusion

It was confirmed that the relaxation strength $\Delta\varepsilon$ and the relaxation time τ for a relaxation process observed around 1MHz in biometric dielectric spectroscopy for the wrist artery increasing during the sprint returned to the resting value obtained before the sprint with the elapsed time. These results indicate an increase in the number of RBCs observed during the sprint and were also confirmed by comparison with the results obtained by ultrasonic blood flow meter and laser blood flow meter. The amount of blood and the number of RBCs increases when a blood vessel dilates for the sprint. The blood flow rate was, however, found to be lower than that at rest because of the dilation of vessels. These results suggest that the blood state in the living body can be observed by dielectric spectroscopy, and even more details in the blood state should be brought from *in vivo* dielectric measurements.

Table.1. Examinee's normal data.

	Gender	Age	Blood Pressure (mmHg)	Pulse (bpm)
A	Male	25	116/74	81
B	Female	33	87/51	62
C	Female	23	88/60	80
D	Male	30	129/62	76
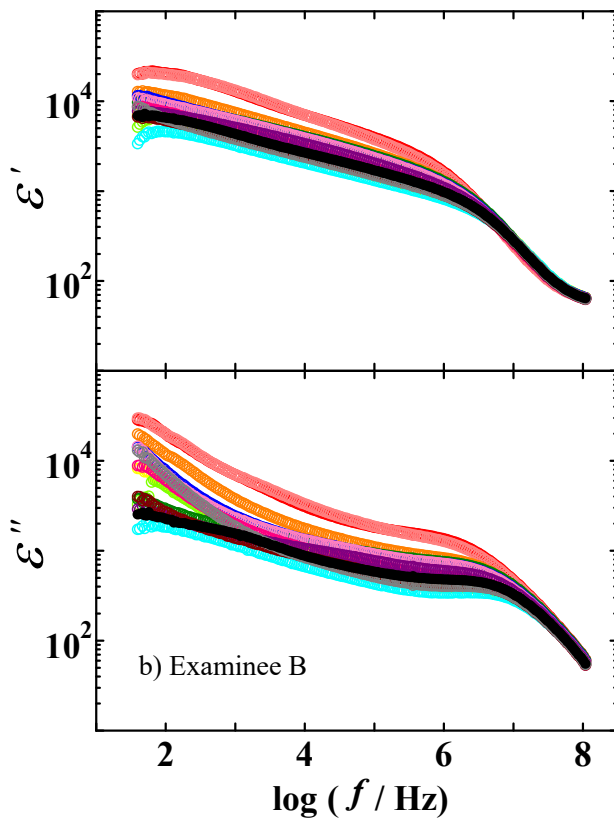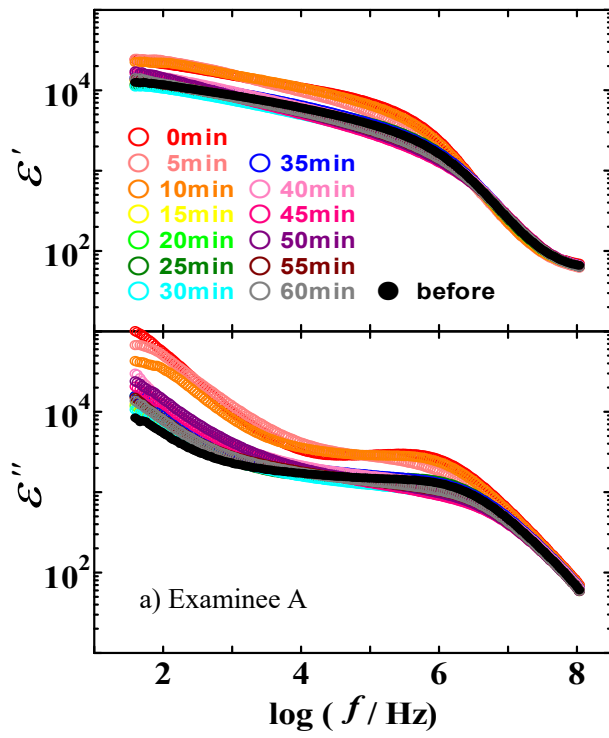
Figure 1. The time dependence of dispersion and loss curves obtained at just above artery of wrist. a) Examinee A, b) Examinee B.
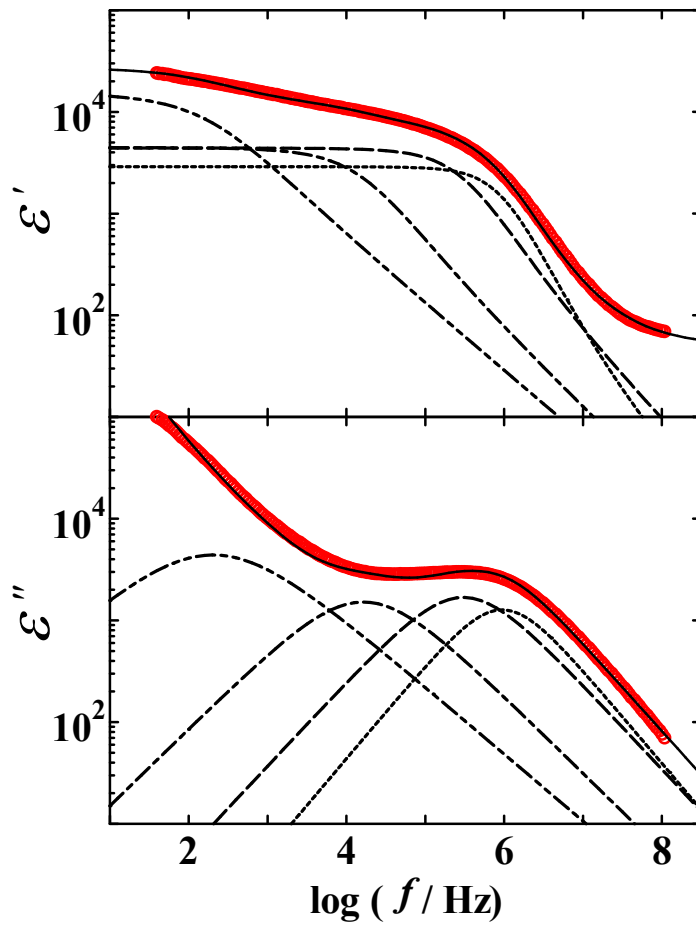
Figure 2. A typical example of the fitting procedure to data for examinee A before the sprint.
Dot line: I-process. Dash line: II-process. Dot-dash line: III-process. Double-dot-dash line:
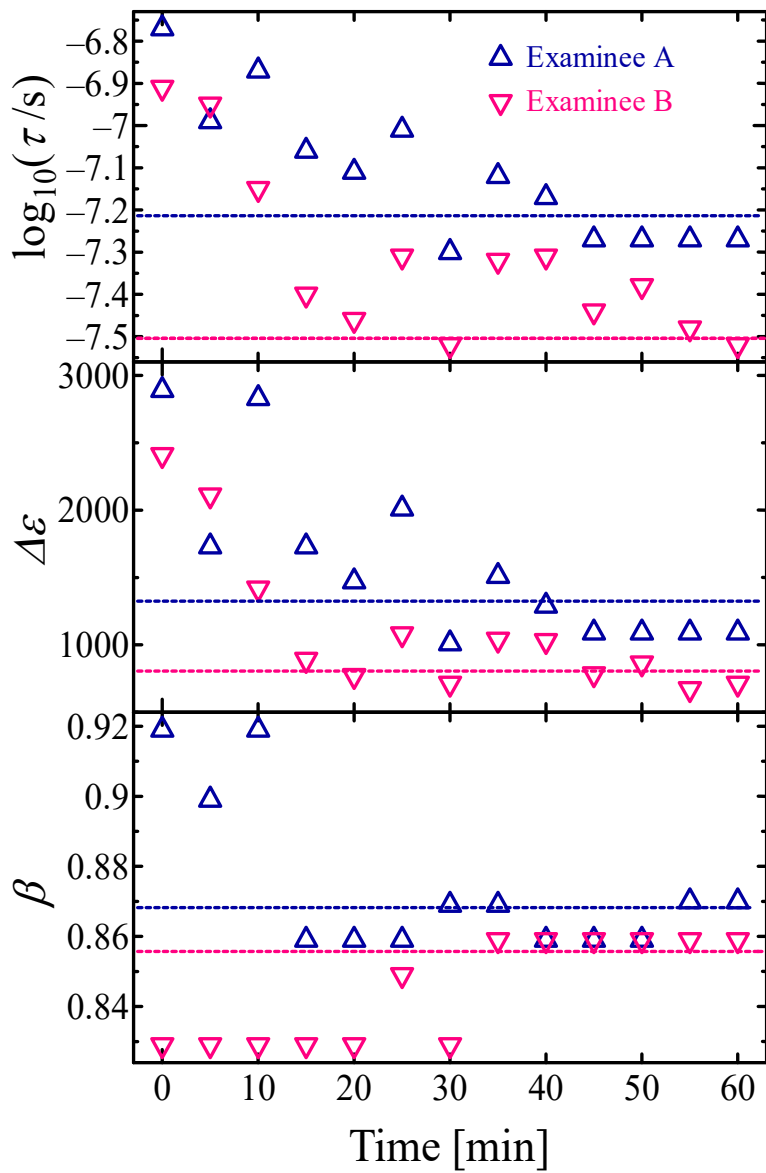IV-process.

Figure 3. Time dependence of the relaxation parameters after the sprint. The dotted lines are the normal data for examinees.
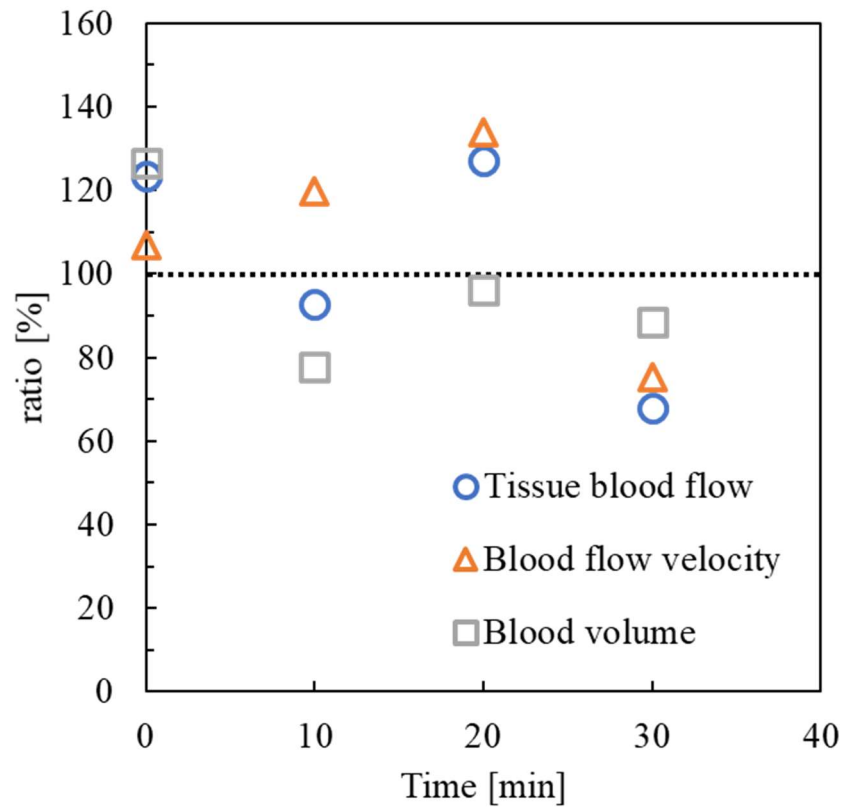
Figure 4. Time dependence of the blood flow parameter ratio for examinee B.
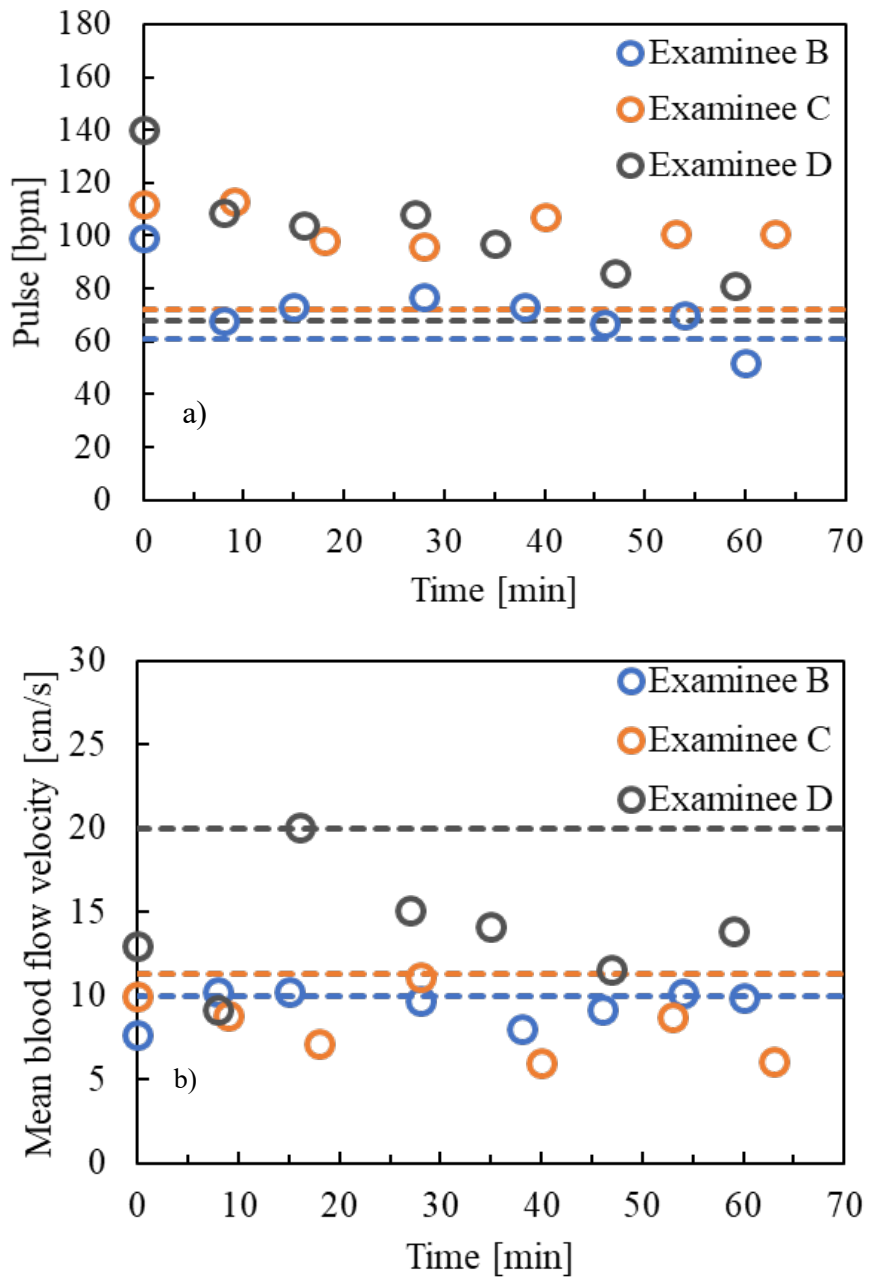
Figure 5. Time dependence of a) the mean blood flow velocity and b) the pulse. The dotted lines are the normal data for each examinee.
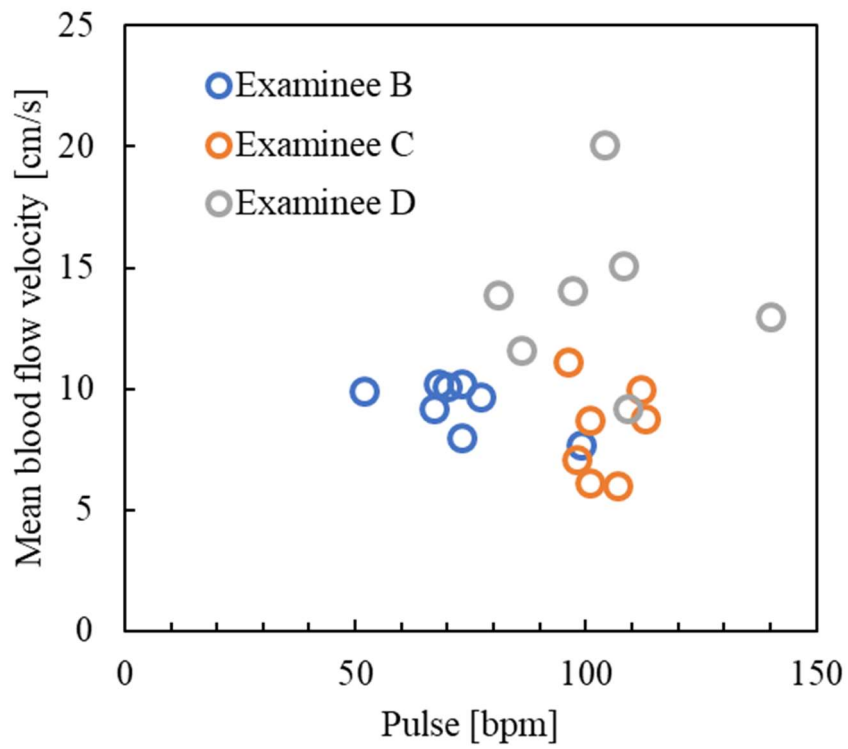
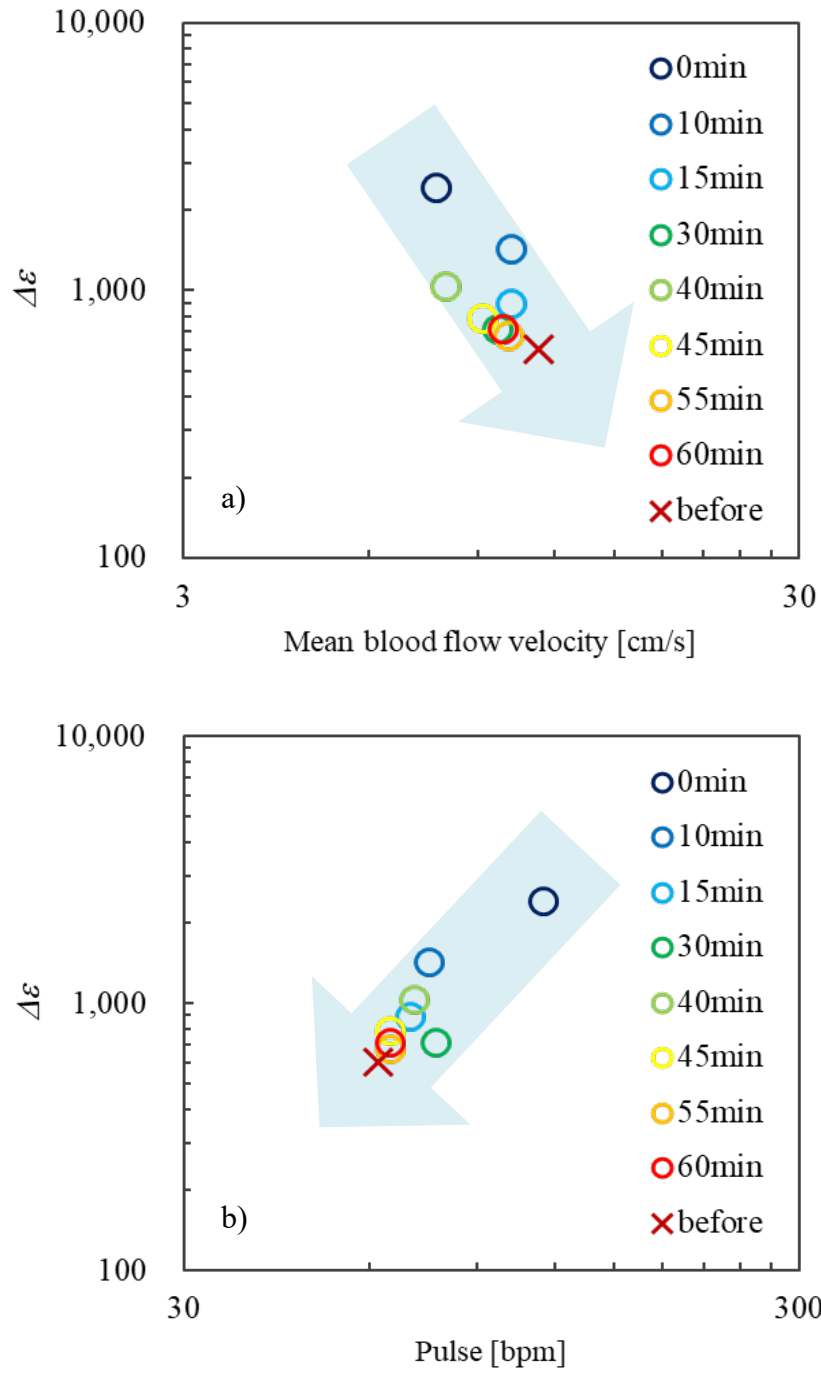Figure 6. The relationship between the pulse rate and the mean blood flow velocity for each examinee.

Figure 7. Comparison of dielectric measurement and ultrasonic blood flow meter
a) mean blood flow velocity and b) pulse.

References

[1] Y. Hayashi, N. Miura, N. Shinyashiki and S. yagihara, Free water content and monitoring of healing processes of skin burns studied by microwave dielectric spectroscopy *in vivo*, Phys. Med. Biol., 50 (2005) 599-612.

[2] T. Hashimoto, M. Yamamura, S. Yagihara, N. Shinyashiki, M. Kazami, I. Uchida, C. Sudou, K. Kouno, T. Arai, S. Osaki and S. Iwagaki, Build up of water in the epidermis after excise, Tokai. J. Sports. Med. Sci., 15 (2003 67-72).

[3] S. Naito M. Hoshi, S. Mashimo, A method of measuring surface permittivity by microwave dielectric analysis, Rev. Sci. Instrum., 67 (1996) 3633-3641.

[4] M. Hashimoto, T. Goto, N. Shinyashiki and S. Yagihara, Interpretation of Hydration Structure of Human Skin from Analysis of Electrodes Used in Dielectric Spectroscopy, Tokai. J. Sports. Med. Sci., 19 (2007) 52-62.

[5] T. Goto, M. Hashimoto, N. Shinyashiki, S. Yagihara and Y. Hayashi, Dielectric study on distribution of water in human skin, Trans. Mat. Res. Soc. Japan., 31 (2006) 771-774.

[6] Y. Feldman, I. Ermolina, Y. Hayashi, Time domain dielectric spectroscopy study of biological systems, IEEE Trans. Dielectr. Electr. Insul., 10 (2003) 728-753.

[7] T. Saito, H. Asano, H. Saito, R. Kita, N. Shinyashiki, and S. Yagihara, in preparation for publication.

[8] S. Kashima, Measurement of tissue blood volume in a model system and in the canine intestine by dynamic light scattering, Lasers. Life. Sci., 6 (1994) 79-90.

[9] K. S. Cole, and R. H. Cole, Dispersion and Absorption in Dielectrics, J. Chem. Phys., 9 (1941) 341-351.

[10] K. Shoji, T. Saito, R. Kita, N. Shinyashiki, S. Yagihara, M. Fukuzaki, T. Ohzono, S. Nishimura, M. Hayashi and H. Tanaka, Dynamics and Aggregate Structuring of Water Molecules in Edible Oil Analyzed by Dielectric Spectroscopy, Trans. Mat. Res. Soc. Japan., 43, 201-204 (2018).

[11] M. A. Lichtman, E. Beutler, T. J. Kipps, and W. J. Williams, "Williams MANUAL OF HEMATOLOGY", 6th Edition, McGraw-Hill Professional (2000), Translated by N. Nara, Medical Sciences International, Ltd., Japan (2003) pp. 3.

Chapter 6

Conclusion

In this thesis, various water structures were discussed with respect to *in vivo* and *in vitro* dielectric spectroscopy measurements. Each chapter treats the observation and analytical techniques of dynamic behavior of water molecules at the characteristic scales of biomaterials in the human body. Details of molecular behavior and interactions discussed in each chapter are summarized here.

In chapter 3, water structures at the molecular level were observed *in vitro* for protein-water mixtures and cheeses. The water structure in aqueous solutions of globular proteins and cheeses containing casein micelles were classified as dispersion systems from fractal analyses using relaxation parameters. However, protein-water mixtures and cheeses were separated into different plot areas. The results of the τ-β diagram indicate that the water molecules are more finely dispersed in cheeses than those in protein-water mixtures. In this way, fractal structure analysis using self-similarity characterized various water structures with complex hierarchical structures. This analytical technique also suggests that water structures related to various biological functions can be characterized along with the dynamic behavior of water molecules determined using dielectric spectroscopy.

In chapter 4, *in vivo* water structures were analyzed using dielectric spectroscopy on the human skin. The penetration depth was determined for each open-ended coaxial electrode with a different diameter from dielectric measurements for a double-layer dielectric model. Measurements of various parts were conducted for two examinees using five different electrode diameters, and the experimental results reflected the thickness of the examinee's epidermis. The experimental results vary depending on the thickness of the epidermis and the water content. Dielectric relaxation measurements of human skin on various parts of the body indicated a low dielectric constant for a part with a large epidermis thickness and little moisture content, while the dielectric constant was high for a part with a small epidermis thickness. These results show that the larger measurement area of the dermis with less skin thickness in terms of penetration depth gives a higher dielectric constant for the dermis with greater moisture content. The state of the examinee's skin can be evaluated by combining the electrode diameter to be used and the measurement parts. The techniques for the *in vivo* measurement of dielectric relaxation for human skin developed here have lead to the evaluation of skin characteristics such as epidermis thickness, water content, and abnormalities due to disease.

In chapter 5, *in vivo* blood flow was observed using dielectric spectroscopy, an ultrasonic blood flow meter, and a laser blood flow meter, and the detailed behavior of the dielectric relaxation was clarified. The MHz frequency processes dominantly attributed to the interfacial polarization of red

blood cells corresponded with the results obtained from both the laser blood flow and the ultrasonic blood flow meters. These detailed *in vivo* evaluations of the blood flow show various possibilities for future applications of these analytical techniques in research areas such as medical and sport science.

Various types of dynamic behavior of hierarchical water structures are treated in this thesis. The order of the length and time scale treated here increases from Chapters 3, 5, and 4. The wide scale of the observation and analysis techniques for molecular dynamics shown here can be realized only with broadband dielectric spectroscopy. The results obtained in this thesis are thus very likely to lead to developments in future research on biological systems. Furthermore, this water structure analysis is not limited to only biological systems, and it is thus expected to expand understanding in various fields in the future.

Research achievements

Publications

1) ◯**Y. Maruyama**, H. Kamata, S. Watanabe, R. Kita, N. Shinyashiki, S. Yagihara, Electric-field penetration depth and dielectric spectroscopy observations of human skin, Skin Research & Technology, in press(accepted).

2) ◯S. Yagihara, R. Kita, N. Shinyashiki, H. Saito, **Y. Maruyama**, T. Kawaguchi, K. Shoji, T. Saito, T. Aoyama, K. Shimazaki, K. Matsumoto, M. Fukuzaki, H. Masuda, S. Hiraiwa, K. Asami and M. Tokita, Physical Meanings of Fractal Behaviors of Water in Aqueous and Biological Systems with Open-Ended Coaxial Electrode, Sensors, 19, 2606 (2019).

3) ◯S. Yagihara, R. Kita, N. Shinyashiki, M. Fukuzaki, K. Shoji, T. Saito, T. Aoyama, K. Matsumoto, H. Masuda, T. Kawaguchi, H. Saito, **Y. Maruyama**, S. Hiraiwa, and K. Asami, Physical Meanings of Fractal Behaviors of Water in Aqueous and Biological Systems, 12th International Conference on Electromagnetic Wave Interaction with Water and Moist Substances (Conference Paper), CFP18IWF-POD, (2018) 8-10.

4) ◯S. Sato, **Y. Maruyama**, H. Kamata, S. Watanabe, R. Kita, N. Shinyashiki, S. Yagihara, M. Egawa, and N. Kunizawa, Evaluation of Water Measurement Techniques for Human Skin by Dielectric Spectroscopy and Confocal Raman Spectroscopy, Transactions of the Materials Research Society of Japan, 40 (2015) 133-136.

5) ◯**Y. Maruyama**, Y. Numamoto, H. Saito, R. Kita, N. Shinyashiki, S. Yagihara, M. Fukuzaki, Complementary analyses of fractal and dynamic water structures in protein–water mixtures and cheeses, Colloids and Surfaces A: Physicochemical and Engineering Aspects, 440 (2014) 42-48.

6) ◯S. Yagihara, Y. Hosoi, S. K. Kundu, T. Kawaguchi, S. Watanabe, H. Kamata, M. Asano, F. Abe, **Y. Maruyama**, S. Sato, H. Saito, Y. Miyamoto, S. Sudo, R. Kita, N. Shinyashiki, M. Fukuzaki, Dynamic Interaction of Electromagnetic Wave with Water Molecules Observed by Broadband Dielectric Spectroscopy and Complementary Experimental Techniques, Proceedings of the 10th International Conference on Electromagnetic Wave Interaction with Water and Moist Substance, (2013) 27-36.

7) ◯**Y. Maruyama**, H. Saito, R. Kita, N. Shinyashiki, S. Yagihara, and M. Fukuzaki, Water Structures in Protein-Water Mixtures Characterized by Dielectric Spectroscopy with Complementary Techniques, Transactions of the Materials Research Society of Japan, 37 (2012) 523-527.

8) ○ **Y. Maruyama**, H. Saito, R. Kita, N. Shinyashiki, S. Yagihara, and M. Fukuzaki, Characterization of Water Structure in Protein-Water Mixtures by Dielectric Spectroscopy and Complementary Approaches, Proceedings of the School of Science of Tokai University, 47 (2012) 115-129.

Presentations

International conferences

1) ◯**Y. Maruyama**, R. Kita, N. Shinyashiki, S. Yagihara, "Water Structure Analysis of Dairy Products by Dielectric Spectroscopy"(Poster), OKINAWA COLLOIDS 2019, Okinawa, Japan, 3-8 November 2019.

2) ◯S. Yagihara, **Y. Maruyama**, H. Saito, T. Kawaguchi, K. Shoji, R. Kita, N. Shinyashiki, and M. Fukuzaki, "Existential state of water molecules in biomaterials"(Oral), The 12th SPSJ International Polymer Conferemce, Hiroshima, Japan, 4-7 December 2018.

3) ◯**Y. Maruyama**, T. Aoyama, R. Kita, N. Shinyashiki, S. Yagihara, "Observation of Dynamic Behavior on Cultured Cells by Dielectric Spectroscopy"(Oral), The 12th SPSJ International Polymer Conferemce, Hiroshima, Japan, 4-7 December 2018.

4) ◯S. Yagihara, K. Shoji, T. Saito, **Y. Maruyama,** H. Saito, R. Kita, N. Shinyashiki, and M. Fukuzaki, "Evaluation of Fractal Water Structures in Various Aqueous Systems by Broadband Dielectric Spectroscopy with Open-end Coaxial Electrodes"(Oral), Progress In Electromagnetics Research Symposium (PIERS 2018), Toyama, Japan, 1-4 August, 2018.

5) ◯**Y. Maruyama**, H. Kamata, R. Kita, N. Shinyashiki, and S. Yagihara, "Non-invasive and Non-destructive Measurements of Human Skin Using Dielectric Spectroscopy"(Oral), Progress In Electromagnetics Research Symposium (PIERS 2018), Toyama, Japan, 1-4 August, 2018.

6) ◯S. Yagihara, R. Kita, N. Shinyashiki, K. Shoji, T. Saito, T. Aoyama, T. Kawaguchi, H. Saito, **Y. Maruyama**, M. Fukuzaki, H. Masuda, S. Hiraiwa, and K. Asami, "Physical Meanings of Fractal Behaviors of Water in Aqueous and Biological systems. The Dispersion of Fragments of Hydrogen Bonding Network"(Oral), 12th International Conference on Electromagnetic Wave Interaction with Water and Moist Substances, Lublin, Poland, 4 June 2018.

7) ◯S. Yagihara, **Y. Maruyama**, H. Saito, Y. Miyamoto, T. Kawaguchi, R. Kita, N. Shinyashiki, and M. Fukuzaki, "New Analytical Method of Water Structures by Fractal Concept"(Oral), IUMRS-ICA2014, Fukuoka, Japan, 24-30 August 2014.

8) ◯S. Yagihara, **Y. Maruyama**, Y. Kishi, R. Kita, N. Shinyashiki, M. Fukuzaki, "Dielectric study on fractal water structures in dispersion systems"(Poster), The 10th International Symposium on Electrokinetic Phenomena (ELKIN 10th), Tsukuba, Japan, 20-24 May 2012.

9) ◯S. Yagihara, **Y. Maruyama**, H. Saito, S. Watanabe, Y. Hosoi, R. Kita, N. Shinyashiki, "Broadband Dynamics of Water Structure in Various Materials"(Oral), IUMRS-ICA 2011 IUMRS 12th International Conference in Asia, 20-22 September 2011.

Japanese conferences

10) ○古旗華保莉, 齋藤徹哉, 斉藤宏伸, <u>丸山裕子</u>, 喜多理王, 新屋敷直木, 八木原晋, "尿素水溶液を塗布したヒト皮膚の誘電測定"(Poster), 第 57 回高分子と水に関する討論会, 東京海洋大学楽水会館大会議室, 2019 年 12 月 3 日.

11) ○S. Yagihara, **Y. Maruyama**, and H. Saito, "Restricted behaviors of solvent molecules in polymer networks evaluated by recent techniques of dielectric relaxation and NMR methods - Gel research in the last 20 years"(Poster), 日本 MRS 創立 30 周年記念シンポジウム, 横浜, 2019 年 11 月.

12) ○S. Yagihara, **Y. Maruyama**, H. Saito, T. Saito, K. Shoji, R. Kita, N. Shinyashiki, and M. Fukuzaki, "Physical meanings of fractal analysis of water structures and recent applications"(Oral), 第 29 回日本 MRS 年次大会, 横浜, 2019 年 11 月.

13) ○**Y. Maruyama**, K. Furuhata, T. Saito, R. Kita, N. Shinyashiki, S. Yagihara, and D. Kurita, "Comparison of Biometric Dielectric Spectroscopy and Blood Flow Measurements"(Oral), 28th Annual Meeting of MRS-Japan 2018, 北九州, 2018 年 12 月 18-20 日.

14) ○S. Yagihara, **Y. Maruyama**, H. Saito, T. Kawaguchi, K. Shoji, R. Kita, N. Shinyashiki, and M. Fukuzaki, "Non-Destructive Testing with Dielectric Spectroscopy Measurements and Fractal Analysis of Water Structures in Moist Materials and Biological Systems"(Poster), 28th Annual Meeting of MRS-Japan 2018, 北九州, 2018 年 12 月 18-20 日.

15) ○<u>丸山裕子</u>, 鎌田隼人, 喜多理王, 新屋敷直木, 八木原晋,"時間領域反射法によるヒト皮膚の誘電測定"(Poster), 第 56 回高分子と水に関する討論会, 東京, 東京海洋大学楽水会館大会議室, 2018 年 11 月 29 日.

16) ○佐藤駿介, <u>丸山裕子</u>, 鎌田隼人, 渡邊精鋭, 喜多理王, 新屋敷直樹, 八木原晋, "Evaluation of Moisture Measurement Techniques for Skin by Dielectric Spectroscopy and Confocal Raman Spectroscopy" (Poster), 第 23 回日本 MRS 年次大会(2013), 横浜, 2013 年 12 月.

17) ○宮本陽介, 山口大貴, <u>丸山裕子</u>, 喜多理王, 新屋敷直木, 八木原晋, "水分子複雑系におけるフラクタル構造のモデリング解析" (Poster), 神奈川県ものづくり技術交流会 (2013), 海老名, 2013 年 10 月.

18) ○斉藤宏伸, 佐々木海渡, 川口翼, 岸泰弘, <u>丸山裕子</u>, 福崎稔, 喜多理王, 新屋敷直木, 八木原晋, "核磁気共鳴および誘電分光法を用いた食品水分の解析手法の構築" (Poster), ものづくり技術交流会, 2012 年.

19) ○山本千晶, 阿部史也, 佐藤駿介, 斉藤宏伸, <u>丸山裕子</u>, 喜多理王, 新屋敷直木, 八木原晋, 福崎稔, 浅野恵美, "誘電分光法による物質・生体の評価" (Poster), ものづくり技術交流会, 神奈川, 2012 年.

20) ○Y. Maruyama, S. Sato, C. Yamamoto, H. Saito, R. Kita, N. Shinyashiki, S. Yagihara, "Human Skin of Various Parts of a Body Observed by Dielectric Spectroscopy"(Poster), 第 22 回日本 MRS 学術シンポジウム, 2012 年 9 月.

21) ○S. Yagihara, H. Saito, Y. Maruyama, R. Kita, N. Shinyashiki, M. Fukuzaki, "Water Structures in Protein Aqueous Systems Characterized by Dielectric Spectroscopy"(Poster), 第 22 回日本 MRS 学術シンポジウム, 2012 年 9 月.

22) ○Y. Maruyama, H. Saito, R. Kita, N. Shinyashiki, S. Yagihara, M. Fukuzaki, "Characterized for Protein-Water Mixtures by Dielectric Spectroscopy and Complementary Approaches", 第 21 回日本 MRS 学術シンポジウム, 2011 年 12 月.

23) ○斉藤宏伸、岸泰弘、<u>丸山裕子</u>、喜多理王、新屋敷直木、八木原晋、福崎稔, "核磁気共鳴法と誘電分光法を用いた分子ダイナミクスの複合的観測"(Poster), 神奈川県ものづくり技術交流会, 2011 年 11 月.

24) ○Y. Maruyama, S. Mibu, R. Kita, N. Shinyashiki, S. Yagihara, "Dielectric Relaxation Measurements and MD Simulations for Protein-Water Mixtures"(Poster), 20th MRS-J Academic Symposium, Yokohama, December 2010.

25) ○八木原晋、喜多理王、新屋敷直木、細井泰之、<u>丸山裕子</u>、渡邉清鋭, "様々な凝集状態をとる混合系における水構造の誘電分光"(Oral), 第 48 回高分子と水に関する討論会, 2010 年 12 月.

26) ○<u>丸山裕子</u>, 細井泰之, 岸泰弘, 壬生早紀, 喜多理王, 新屋敷直木, 八木原晋, "タンパク質‐水系とリポソーム‐水系における水構造のマイクロ波誘電緩和測定" (Poster), 神奈川県ものづくり技術交流会, 海老名, 2010 年 10 月.

27) ○細井泰之, 松本佳祐, <u>丸山裕子</u>, 喜多理王, 新屋敷直木, 八木原晋, "誘電緩和測定によるリポソームー水系の動的挙動に関する研究" (Poster), 第 32 回日本バイオレオロジー学会年会, 2009 年 6 月.